Homogenization of the Stellar Population along Late–Type Spiral Galaxies[1]

D. A. Gadotti
Departamento de Astronomia, Instituto Astronômico e Geofísico, Universidade de São Paulo
Avenida Miguel Stefano, 4200, São Paulo – SP, Brasil, CEP 04301-904
dimitri@iagusp.usp.br

and

S. dos Anjos
Departamento de Astronomia, Instituto Astronômico e Geofísico, Universidade de São Paulo
Avenida Miguel Stefano, 4200, São Paulo – SP, Brasil, CEP 04301-904
sandra@iagusp.usp.br

ABSTRACT

We present a study of the broadband UBV color profiles for 257 Sbc barred and non–barred galaxies, using photoelectric aperture photometry data from the literature. Using robust statistical methods, we have estimated the color gradients of the galaxies, as well as the total and bulge mean colors. A comparative photometric study using CCD images was done. In our sample, the color gradients are negative (reddish inward) in approximately 59% of the objects, are almost null in 27%, and are positive in 14%, considering only the face–on galaxies, which represents approximately 51% of the sample. The results do not change, essentially, when we include the edge–on galaxies.

As a consequence of this study we have also found that barred galaxies are over–represented among the objects having null or positive gradients, indicating that bars act as a mechanism of homogenization of the stellar population. This effect is more evident in the (U−B) color index, although it can also be detected in the (B −V) color.

A correlation between the total and bulge colors was found, which is a consequence of an underlying correlation between the colors of bulges and disks found by other authors. Moreover, the mean total color is the same irrespective of the gradient regime, while bulges are bluer in galaxies with null or positive gradients, which indicates an increase of the star formation rate in the central regions of these objects.

We have also made a quantitative evaluation of the amount of extinction in the center of these galaxies. This was done using WFPC2 and NICMOS HST archival data, as well as CCD B, V and I images. We show that although the extinction in the

[1]Based partly on observations made at the Pico dos Dias Observatory (PDO/LNA – CNPq), Brazil

V–band can reach values of up to 2 magnitudes in the central region, it is unlikely that dust plays a fundamental role in global color gradients.

We found no correlation between color and O/H abundance gradients. This result could suggest that the color gradients are more sensitive to the age rather than to the metallicity of the stellar population. However, the absence of this correlation may be caused by dust extinction. We discuss this result considering a picture in which bars are a relatively fast recurrent phenomenon.

These results are not compatible with a pure classical monolithic scenario for bulge and disk formation. On the contrary, they favor a scenario where both these components are evolving in a correlated process, in which stellar bars play a crucial role.

Subject headings: galaxies: evolution — galaxies: formation — galaxies: spiral — galaxies: statistics — galaxies: stellar content — galaxies: structure

1. Introduction

Several recent works have been contributed to our understanding of the dynamical evolutionary processes related to stellar bars in galaxies (see Friedli 1999 for a review). Much of these works point to the possibility that these processes may be related to the formation and/or building of galactic bulges, as opposed to a pure monolithic scenario (Eggen, Lynden–Bell & Sandage 1962) and the hierarchical scenario (e.g., Kauffmann & White 1993, Kauffmann, Guiderdoni & White 1994, Baugh, Cole & Frenk 1996, Bouwens, Cayón, & Silk 1998).

We know that bars are very easy to form in stellar disks due to non–circular orbits of the stars in the disk, or due to instabilities generated by the presence of a companion. In the RC3 (G. de Vaucouleurs et al. 1991), for instance, 30% of the spiral galaxies are strongly barred. Recent theoretical studies based on N–body simulations (e.g., Friedli & Benz 1995 and references therein) show that, once formed, the stellar bar induces a series of dynamical processes in the host galaxy. Basically, these studies show two routes for the formation and/or building of galactic bulges. In the first one, stellar bars could collect gas from the outer disk, generating bursts of star formation and a chemical enrichment in the central regions. Another possibility is that the stars themselves might be transported from the disk to the bulge, through, for instance, the hose mechanism (Toomre 1966), orbital resonances (Combes & Sanders 1981) and the onset of irregular stellar orbits (e.g., Berentzen et al. 1998). Moreover, Norman, Sellwood & Hasan (1996), among other theoretical works, showed that the central concentration of mass, induced by the bar, could destroy its orbital structure and eventually the bar itself. These authors suggest that the formation of the bar, its dissolution and consequent formation and/or building of the bulge, may be a fast recurrent process (i.e., $\sim 10^8$ years). Friedli & Martinet (1993) suggest that the continuous building of the bulge in a galaxy could actually change its overall morphology. One Sc

galaxy, for instance, might become in a first step a SBb, and then a Sb, giving an evolutionary meaning to the late–type spiral scheme along the Hubble sequence.

From the observational point of view, comparative studies related to the general properties of barred and non–barred galaxies seem to give some support to the formation and/or building of galactic bulges through this secular evolutionary scenario. Kormendy (1982) found that triaxial bulges, which are normally associated with bars, rotate faster than bulges of non–barred galaxies. Kormendy & Illingworth (1983) showed that bulges of barred galaxies have a central velocity dispersion smaller than the one presented by bulges in non–barred galaxies. Martin & Roy (1994) and Zaritsky, Kennicutt & Huchra (1994) show that barred galaxies have less pronounced O/H gradients than non–barred galaxies. Sakamoto et al. (1999) show that barred galaxies present a higher degree of central concentration of CO molecular gas than non–barred galaxies.

Moreover, box–shaped bulges, representing at least 20–30% of edge–on S0's (de Souza & dos Anjos 1987, Shaw 1987), seem to show this morphology as a consequence of steps in the secular dynamical evolutionary processes in bars, as indicated by a series of recent results (Kuijken & Merrifield 1995, Merrifield & Kuijken 1999, Bureau & Athanassoula 1999, Athanassoula & Bureau 1999, Bureau & Freeman 1999, Bureau, Freeman & Athanassoula 1999).

Studies related to general properties of spirals (e.g., Peletier & Balcells 1996) revealed similar broadband colors of the inner disk and bulge; Courteau, de Jong & Broeils (1996) and de Jong (1996b) found a correlation between the scale lengths of disks and bulges. These results indicate the existence of an evolutionary connection between these two components (see Wyse, Gilmore & Franx 1997 for a review), and have been interpreted as a consequence of the dynamical secular evolutionary scenario.

Another way to obtain clues related to the formation and evolution processes in galaxies is through the study of radial color distribution. However, surprisingly, there are few statistical works in the literature exploring the broadband colors to study the bulge and the disk components separately. The study of the integrated broadband colors in galaxies have been done to obtain information concerning the stellar population (e.g., Searle, Sargent & Bagnuolo 1973, Tinsley 1980, Frogel 1985, Peletier 1989, Silva & Elston 1994), as well as the internal extinction caused by the interstellar dust (e.g., Evans 1994, Peletier et al. 1994). Exceptions are the works of de Jong & van der Kruit (1994) and de Jong (1996a), for instance. Such studies certainly bring clues about the bulge formation scenarios.

The main goal of this paper is to compare the color gradients' behaviour in barred and non–barred late–type galaxies and verify if these results are in agreement with the predictions from evolutionary processes. A very fast way to verify alternative scenarios for the formation and/or building of bulges, exploring the radial color distribution in a statistical point of view, is to use the available data in the literature.

With this objective, we have selected a sample of 257 Sbc galaxies with broadband colors available in the literature and observed through photoelectric aperture photometry (Sect. 2).

Using robust statistical methods, we estimated, for each galaxy, the color gradient as well as the mean total and bulge characteristic color indices (Sect. 3). Moreover, we have also acquired CCD images for 14 galaxies in the sample (Sect. 4) in order to test the accuracy of our results. In Sect. 5 we present the main results of our analysis and, finally, in Sect. 6 we present a general discussion and our main conclusions.

2. Sample Selection

The photoelectric data used in this analysis were extracted from the compilation by Longo and A. de Vaucouleurs (1983) and its supplement (Longo & A. de Vaucouleurs 1985). Both compilations will hereafter be referred to as LdV83,85, respectively. Among other information, the catalogue presents for different galaxies the (U−B) and (B −V) aperture color indices extracted from the literature. We have selected galaxies with Hubble stage index T = 3, 4 or 5, corresponding to morphological types Sb, Sbc and Sc, barred and non–barred, and having B_T brighter than 14, according to the Third Reference Catalogue (G. de Vaucouleurs et al. 1991; hereafter RC3). This criterion assures that the morphological classification is more reliable, since fainter objects are, in general, more difficult to be classified. Nevertheless, it is worth notice that several galaxies were distinctly classified in the LdV83,85 and in the RC3. Since the rms uncertainty associated with the morphological type is of order 2 units (Lahav et al. 1995), we will consider all galaxies in our sample as belonging to one unique mean morphological class (T = 4 ± 1).

We remark that our choice for galaxies in this specific type range was motivated by the fact that these are the most luminous objects in the B broadband along the Hubble sequence (van den Bergh 1997, Roberts & Haynes 1994). This is possibly indicating that these systems have the highest rate of star formation among spirals. Another reason for this choice comes from the observation that it is possible that the dynamical evolutionary processes occur mainly in late–type spirals rather than in early–type ones (Wyse, Gilmore & Franx 1997).

A first selection of the data was partially done with the electronic version of the catalogue, available at the CDS (*Centre de Données Astronomiques de Strasbourg*), and resulted in a sample containing 531 objects. In order to have an equally representative set of data, we have removed from the sample those objects with less than 5 different color aperture data. Thus, we selected only those objects for which a more careful study of the distribution of the color indices could be done.

We know that extinction by dust can strongly affect studies of the radial color distribution in the U, B and V bands, in particular for late–type galaxies. However, these bands are well suited for the study proposed here, since in these bands we can detect recent star formation, which is a possible consequence of the dynamical secular evolutionary scenario. In order to minimize the effects of dust, we have also performed a visual inspection of all galaxies, using images of the DSS (Digitized Sky Survey), eliminating those peculiar systems, (e.g., NGC 891), presenting clear

perturbations, such as strong dustlanes or close companions in strong interaction, that could disturb the analysis. After this last step we ended with a final sample having 257 galaxies, used in the present analysis.

3. Estimating Gradients and Colors

3.1. Color Gradients

As mentioned before, we have used the LdV83,85 data to estimate the (U−B) and (B −V) color gradients of the galaxies in our sample. Since this is a compilation of data acquired by different observers, telescopes, instruments and in different atmospheric conditions, it is natural that, for any given galaxy, some data will not appear consistent, due to larger internal errors. For instance, different authors could assign quite distinct values for the color index of the same galaxy at the same aperture. Indeed, this is the case, for example, of NGC 2377 in the aperture of 2.6 arcminutes, where three different sources gave to the (U−B) color index the values 0.11, 0.20 and 0.38! Therefore, trying to fit a straight line to the color data, using these discrepant values and the classical least squares regression (LS), will result in a quite uncertain estimative for the color gradient.

Since we do not know a priori how to identify the bad data, it is mandatory to use some robust statistical technique more insensitive to the presence of these uncertainties. In our analysis, we choose to apply the Least Median of Squares (LMS) method (Rousseeuw 1984). Contrary to the classical LS regression, this method minimizes the *median* of the squared residuals. The results obtained are more resistant to the effects of contamination in the data. More specifically, the estimation of the color gradient was done with the program PROGRESS (Rousseeuw & Leroy 1987), available at the StatLib (http://www.lib.stat.cmu.edu/). This program performs a robust regression analysis by means of the LMS method, yielding more reliable estimates of the regression parameters, and allowing to identify outliers in the data. PROGRESS first calculates the regression parameters by LS, then by LMS, and finally by a reweighted LS (in which the outliers have weight zero). Through this algorithm, the estimated gradient has, in most cases, the same value obtained through the LMS method alone. However, the reweighted LS method works better than the LMS method when the number of data points is small (Rousseeuw 1984, Rousseeuw & Leroy 1987).

The color gradient was estimated following the same definition of Prugniel & Héraudeau (1998), i.e.,

$$G = \frac{\Delta(X - Y)}{\Delta \log A}, \tag{1}$$

where $(X - Y)$ represents the integrated color index in magnitudes within an aperture A in units of 0.1 arcminute.

The estimation of each gradient was also accompanied by a graphical visual inspection, since, in some cases, the results from the non–reweighted LS were more representative than those by LMS or by the reweighted LS. This could happen because, when trying to minimize the errors, the LMS method can be fooled by a small group of data points that fits very well a straight line. Thus, in these cases, we defined the gradient by the parameters obtained by the classical LS regression.

From our sample of 257 galaxies, we obtained 239 (B −V) and 202 (U−B) color gradients. The other estimations were rejected either because the number of data points were too small and/or the points were too inconsistent to result in a reliable value. Figure 1 shows four examples of the radial color distribution in galaxies. NGC 1425 and NGC 2613 are examples of objects having the more typical negative color gradient. An example of object with a clear null gradient is NGC 1672. The more rare case of objects with a positive gradient is represented here by UGC 3973. In this figure, we can also compare the fits using the three different methods discussed above. The dashed lines refer to the standard LS method, while dotted lines refer to the LMS method and the solid lines refer to the PROGRESS algorithm. Note the importance of using a robust statistical method to determine color gradients in such cases as for NGC 2613 and UGC 3973.

The LdV83,85 data is not corrected for either Galactic reddening or internal reddening. In determining the color gradients, the correction for Galactic reddening is not necessary, since it only introduces a constant vertical shift of the points, not affecting the gradient evaluation. However, the correction for internal reddening is quite difficult to predict correctly, due to the still unsolved problems related to the optical thickness and the inclination of galaxies (e.g., Giovanelli et al. 1995, de Jong (1996c)). However, although such a correction could be important for any particular object, it will only produce minor changes compared to the uncertainties involved in the measurement and determination of the color gradients.

On the other hand, in models of the dust distribution in disk dominated galaxies, it was shown (de Jong (1996c)) that only a small fraction of the color gradients could be due to dust reddening, i.e., dust reddening plays a minor role in color gradients. Furthermore, color gradients induced by dust are small from U to R broadbands, because the absorption properties do not change very much among these bands.

In Fig. 2 we show the color gradients plotted against both the Galactic reddening and the inclination of the galaxies. We can see from this figure that the two corrections mentioned above do not interfere with the distribution of color gradients obtained in our sample. The top panels show that there is no correlation between color gradients and Galactic reddening, represented by the color excess $E(B-V)$, determined through the recently obtained maps of Schlegel, Finkbeiner & Davis (1998). On the other hand, since the internal reddening varies with the inclination of the galaxy along the line of sight, which can be represented by the $\log R_{25}$ parameter of the RC3, the bottom panels of Fig. 2 show that there is no clear correlation between color gradients and internal reddening. Since no correlation was found, we opt to neglect the internal reddening when estimating the color gradients. We remark, however, that both effects are still obviously relevant

when dealing with the integrated color, as we present in the next subsection.

3.2. Total and Bulge Colors

We have used two different procedures to determine the total and the bulge characteristic color indices. In the first one, we adopt the bulge color as the one observed through the smallest aperture, and the total color as the one observed through the aperture that reaches the 25 mag arcsec^{-2} B isophotal level, as presented in the RC3. In some cases, when the data do not reach the dimensions required, an extrapolation was done using the estimated gradient. On the other hand, an average was done for apertures with several data points. No reddening corrections were made in this method.

We stress that this method is completely unbiased, in the sense that we use the original data, and therefore it is useful to verify if the total colors and the colors of bulges are correlated. Such correlation should in fact exist, since the colors of bulges and disks are correlated (Peletier & Balcells 1996). They have used the (U−R), (B−R), (R−K) and (J−K) colors in a sample of 30 early–type spirals (earlier than Sbc). As shown in Sect. 5.5, we also found a good correlation, consistent with the findings of these authors.

Since galaxies have different angular sizes and were observed through different sets of apertures, the method described above is only an approximated procedure, since, in many cases, the measurements were made at different galactocentric distances. In order to compare the data of galaxies at the same physical dimension, we have defined a characteristic bulge color index as the one measured within 1/5 of the galaxy effective radius. Even if there is some disk contamination at this aperture, the major contribution comes from the bulge, and therefore we made no attempt to correct for this contamination. Using the definition of gradient (Eq. (1)), this bulge color was derived from our fits as

$$(X-Y)_b = (X-Y)_{eff} - 0.7G, \tag{2}$$

where $(X-Y)_{eff}$ is the effective color index, measured within the effective aperture in the B band. We have also define a characteristic total color as the one measured within 2 effective radius, corresponding therefore to

$$(X-Y)_T = (X-Y)_{eff} + 0.3G. \tag{3}$$

Equations (2) and (3), and the effective color indices given by the RC3, were used to determine these characteristic colors.

As we have already mentioned, this second method is more suitable to compare the values from different galaxies. However, we could not use this method to verify the correlation between

the total colors and the colors of bulges, since Eq(s). (2) and (3) already imposes such a correlation, as one can see by subtracting them. Therefore, this justifies our first rough method used only to verify the existence of a real correlation, since that method do not suffer from this kind of bias.

We have corrected these characteristic color indices for Galactic reddening using the maps of Schlegel, Finkbeiner & Davis (1998) to obtain the (B −V) color excess, and used the relation

$$\frac{E(U-B)}{E(B-V)} = 0.72 \pm 0.03, \tag{4}$$

which can be found in Kitchin (1998).

We did not correct these values for any differential internal reddening between bulge and disk. Instead, we have applied an integrated correction to account for the effects of inclination. According to Giovanelli et al. (1994), the internal extinction as a function of the inclination of the galaxy, derived from I–band images of Sc galaxies, is

$$A_I = 1.12(\pm 0.05) \log \frac{a}{b}, \tag{5}$$

where a and b are, respectively, the major and minor axis of the galaxy. For the U, B and V bands, Elmegreen (1998) shows that the extinction coefficients are, respectively, 3.81, 3.17 and 2.38 times the extinction coefficient in the I band, according to observations done in the Galaxy. Since the Galaxy is likely a Sbc galaxy we used these same relations for the objects in our sample. Using the definition of the color excess and the fact that $\log a/b$ is approximately equivalent to the $\log R_{25}$ parameter of the RC3, we finally arrive to the relations used in our work:

$$E(U-B) = 0.68 \log R_{25} \tag{6}$$

and

$$E(B-V) = 0.87 \log R_{25}. \tag{7}$$

It is interesting to observe that the corrections we have applied are actually $\sim$ 2–3 times larger than the ones adopted in the RC3! Indeed, earlier works (see, e.g., G. de Vaucouleurs 1959) argued that spiral galaxies were nearly transparent. But more recent studies (e.g., Boselli & Gavazzi 1994, Giovanelli et al. 1995) show that the optical thickness of spiral galaxies is higher. The adopted corrections in Eq(s). (6) and (7) assume that spiral galaxies have a large optical thickness, and thus are much more realistic.

Although the galaxies in our sample can be considered as local (-295 Km/s (NGC 224) $\leq cz \leq$ 8720 Km/s (UGC 4013)), with a typical value of $cz \sim 2000$ Km/s), we have also applied the K–correction, using the equations of the RC3.

The galaxies analyzed in this work, as well as the results from the determination of the (B −V) and (U−B) gradients, and of the total and bulge color indices, can be seen in Table 1.

4. Comparative Studies

4.1. CCD Images

The ideal set of data to study the radial color distribution in the disk and bulge components is obtained by using CCD photometry, which permits a differential evaluation of the color along the galaxies. However, as mentioned before, we have choose a more fast way in order to have a statistically significant set of data. This was the main reason which lead us to use the available data from LdV83,85. It is interesting, therefore, to compare the color distribution obtained from CCD and aperture photoelectric photometry.

In this subsection, we present a comparison with the CCD data of 14 galaxies observed at the Pico dos Dias Observatory (PDO/LNA – CNPq, Brazil). The CCD observations were done with a 24 inch telescope having a focal ratio f/13.5, and using a thin back–illuminated CCD SITe SI003AB, with 1024 × 1024 pixels. The plate scale is 0.57 arcsec/pixel, resulting in a field of view of approximately 10 × 10 arcmin. The CCD gain was fixed on 5 electrons/ADU and the read–out noise on 5.5 electrons. All objects were observed in the B, V, R and I passbands of the Cousins system. For each object, we have done 6 exposures in the B band, 5 in the V, and 3 in the R and I bands, typically, with an exposure of 300 seconds. The multiple exposures aim to ease cosmic ray removal. The data was calibrated with a set of standard stars of Graham (1982) and corrected for atmosphere and Galactic extinction. The later correction was done using the maps of Schlegel, Finkbeiner & Davis (1998).

The standard processing of the CCD data includes bias subtraction, flatfielding and cosmetics. The first step in the sky subtraction was done by editing the combined images in each filter, removing the galaxy and stars. After that step we determined the mean sky background and its standard deviation (σ). Then, we removed all pixels whose values were discrepant by more than 3 σ from the mean background. An sky model was obtained by fitting a linear surface to the image, and this model was subtracted from the combined image. We finally removed objects such as stars and HII regions. All these procedures were done using the IRAF[2] package.

We then used the ELLIPSE task to calculate the surface brightness profiles of each galaxy in each band. Subtracting the profiles we obtained color gradients, constructing tables in the same units of the ones in LdV83,85. These tables were used in the PROGRESS algorithm to provide values for the gradients in the same way it was done for our whole sample.

[2]IRAF is distributed by the National Optical Astronomy Observatories, which are operated by the Association of Universities for Research in Astronomy, Inc., under cooperative agreement with the National Science Foundation.

In Fig. 3, we show a plot of the CCD gradients and those obtained with the photoelectric aperture data, showing that both estimations are essentially the same. The good correlation between these two set of values (Pearson correlation coefficient R = 0.93) gives support to the results obtained with the LdV83,85 data. The mean difference is $G_{LdV} - G_{CCD} \simeq -0.06$.

We have also done a comparison with the CCD observations made by de Jong & van der Kruit (1994) to study color profiles in a sample of 86 face–on disk galaxies. We have applied for the 8 galaxies our samples have in common, the same method we have used in this work, using the B and V CCD images kindly provided by de Jong. We have simulated photometric apertures on these images using the IMEXAMINE task from IRAF. The comparison of the (B −V) gradients obtained using the photoelectric data by LdV83,85 and de Jong's CCD images revealed a Pearson correlation coefficient of $R = 0.74$. If we do not consider two outliers the Pearson coefficient is $R = 0.97$.

4.2. Comparison with Prugniel & Héraudeau

Prugniel & Héraudeau (1998), hereafter PH98, have also estimated the (U−B) and (B −V) gradients, using both CCD and photoelectric aperture photometry, for a large fraction of the galaxies in our sample. To avoid the uncertainties due to inconsistent measures these authors have attributed different statistical weights to each source of data.

In Fig. 4 we present a comparison between the gradients determined in the present work and those estimated by PH98. The correlation coefficient R is 0.85 for (B −V) and 0.81 for (U−B). Moreover, we can see that there are no systematic differences between the two works. The mean value of the differences is 0.004 in (B −V) and 0.011 in (U−B).

5. Analysing Gradients, Colors and Bars

In this section, we will analyse the results obtained from Sect. 3, regarding the color gradients, as well as those relating to the total and bulge color indices. We have separated our sample into barred (SAB+SB) and non–barred (S+SA) galaxies, in order to test the bulge formation in the evolutionary and monolithic scenarios. Since the identification of bars is much more difficult in edge–on systems, and the effects of dust extinction are minimized in face–on galaxies, we took the special care of analysing the face–on and the edge–on galaxies separately. We use the same criterion as de Jong & van der Kruit (1994), defining as face–on those galaxies with $\log R_{25} \leq 0.20$, corresponding to $b/a \geq 0.625$. Galaxies which do not obey this criterion we regard as edge–on. The following galaxies, IC 983, NGC 253, NGC 1169, NGC 1625, NGC 1964, NGC 2276, NGC 2377, NGC 2525, NGC 3344, NGC 3646, NGC 4394, NGC 4402, NGC 5054, NGC 6215, NGC 6300, NGC 6878A, NGC 7307 and UGC 11555, whose gradients were too uncertain to be used, were removed from our sample.

Table 1 shows the color gradients and its errors for all galaxies in our sample, as well as the bulge and total characteristic color indices. The errors of the gradients are the ones obtained through the PROGRESS algorithm and thus are fit errors, which are larger than the photometric errors alone. One can see that the mean error on the (B −V) gradient is 0.03, and on the (U−B) is 0.05. The mean errors for the bulge and total color indices are, respectively, 0.04 and 0.03 for (B −V) and 0.05 and 0.04 for (U−B).

5.1. Gradients' Distributions

The distribution of the color gradients for barred and non–barred galaxies, considered separately, both face and edge–on projections, can be seen in Fig. 5. The statistical data from this figure are presented in Table 2, where column (1) contains the description of each subsample, while columns (2) and (5) contain the total number of objects in each subsample in each color index. Columns (3) and (6) show the mean values and their respective standard errors. Finally, columns (4) and (7) contain the standard deviations of these distributions. These values were obtained through a Gaussian fit to the observed distribution.

We can observe from Fig. 5 that the (U−B) distribution for barred galaxies, for both the face and edge–on projections, is wider than the distribution for non–barred galaxies. The results in Table 2 also show that barred galaxies have wider distributions. From this table, we can see that the differences in the standard deviations are larger than the expected photometric errors, indicating that this is indeed a real effect. With a smaller amplitude, the same effect is also present in the (B −V) gradients. Even considering that the photometric errors are larger in the U band, this can hardly explain this effect since such errors affect both kinds of objects, barred and non–barred, in the same way. Therefore, this is a real characteristic of barred galaxies, namely, to present a larger interval of (U−B) color gradients, probably associated with recents episodes of star formation. We note that the larger distributions are caused by a larger fraction of barred galaxies having zero or positive gradients. In (U−B), for instance, 55% ± 8% of the face–on barred galaxies have zero or positive gradients, whereas for the face–on non–barred galaxies this fraction is reduced to 32% ± 12%. However, considering the (B −V) index, these fractions are more similar, being 41% ± 6% among barred galaxies and 31% ± 11% among non–barred galaxies. At this point we might suspect that this difference between the two color indices may be caused by a larger age/metallicity sensibility of the (U−B) color index. We remark that this effect is present even when we do not separate the edge and face–on galaxies.

Moreover, one can see in Fig. 5 that the majority of barred galaxies have less pronounced (U−B) gradients than the non–barred galaxies, as can be also verified through the mean values presented in Table 2. But, interestingly, this behaviour does not occur in the (B −V) color. This is probably an effect that any enhancement in the star formation rate affects more the (U−B) than the (B −V) color.

Another interesting effect is that the edge–on galaxies show a tendency of having more pronounced negative gradients compared to the face–on systems, specially in (U−B). This effect may well be related to the fact that the internal reddening is more expressive in edge–on galaxies, and points to the presence of a small differential internal correction that affects the bulge and the disk in different ways. Indeed, one can conclude that the light emitted by the central regions shall be more affected by reddening, a result that agrees with the ones presented by de Jong (1996c).

We present in Fig. 6 the (U−B) versus the (B −V) gradients for the non–barred galaxies (a), barred galaxies (b) and for the total sample (c). We can see from this figure that the gradients in both colors are well correlated, and that there is no difference in the correlation for barred and non–barred galaxies. In fact, the Pearson correlation coefficient R is 0.71 for non–barred, 0.80 for barred, and 0.78 for the whole sample. The same correlation was observed separating face and edge–on galaxies without noticeable differences. Again, we can see that barred galaxies have a more extended color gradient amplitude in these plots. These correlations are indeed expected, since the same physical reason rules the gradients in both colors, namely, variations between the stellar populations of the inner and outer regions of the galaxies. The models of Larson & Tinsley (1978), for instance, show that, for a population formed in a single burst, the variation in (B −V) for populations with a difference in age of 10 Giga years is 1.1, while for (U−B) it is 1.5. Thus, in these conditions, we shall expect $\Delta(U-B)/\Delta(B-V) = 1.4$. Since the color gradients are $G_{B-V} = \Delta(B-V)/\Delta \log A$ and $G_{U-B} = \Delta(U-B)/\Delta \log A$, then we shall have $G_{U-B}/G_{B-V} = 1.4$. Surprisingly, the correlations in Fig. 6 give us $G_{U-B}/G_{B-V} = 1.2$, which is very close to what is predicted from these simple models. This difference might indicate that we are seeing stellar populations mixed with dust, since Larson and Tinsley's models do not take dust into account.

Thus we interpret that the reason for this agreement, as will be seen in Sect. 5.5, is that the total color index is relatively stable among galaxies in our sample, but the color of the bulge varies noticeably between the barred and non–barred populations. Therefore, the amplitude of variation in the color gradients shown in Fig(s). 5 and 6 is related to variations in the stellar population of the bulges.

It is interesting to ask what would happen if the weakly–barred galaxies (SAB's) would have been analysed separately. The answer to this question is the analysis would remain the same. Indeed, barred and weakly–barred galaxies show essentially the same mean color gradient in both the (B −V) and (U−B). The values for barred galaxies alone are -0.12 ± 0.02 and -0.11 ± 0.03, respectively, while for the weakly–barred galaxies these values turn to -0.14 ± 0.02 and -0.13 ± 0.03.

5.2. Negative, Zero and Positive Gradients

The vast majority of the galaxies in our sample have negative gradients, as one can see from Fig. 5, implying therefore that the bulge is redder than the disk. This result, in principle, is consistent with the monolithic scenario, where the older and redder population is located in the central parts, whereas the younger and bluer populations are more predominant in the outer regions of spiral galaxies.

In order to get some further insight, we have considered three arbitrary categories for the color gradients, according to their values. The first category is constituted by objects having negative gradients, with $G \leq -0.10$; the second have galaxies with almost zero gradient, defined by $-0.10 < G < 0.10$, and finally the third category have those galaxies with positive gradients, $G \geq 0.10$. In Table 3 we show for the face–on galaxies in our sample, where the distinction between barred and non–barred is more reliable, the distribution among these three classes of objects, in both colors. There are a total of 124 face–on galaxies with the (B −V) gradient, and 104 with the (U−B). In column (1) we present the total number of galaxies in each class of color gradient, while column (2) gives their fraction of the total sample. Column (3), (4) and (5) show, respectively, the fractions of non–barred, weakly–barred and barred galaxies in each gradient interval. Column (6) shows the total fraction of barred (SAB+SB) galaxies and, finally, Column (7) shows the number of galaxies hosting AGN's. Galaxies with AGN were identified through the catalog of Véron–Cetty & Véron (1998). The reason to investigate this class of galaxies in this study comes from the suggestions presented by other authors (e.g., Shlosman, Frank & Begelman 1989, Shlosman, Begelman & Frank 1990) that bars can fuel AGN through processes similar to the ones of the secular evolution. We can verify that, with small variations in each color index, we have approximately 59% of the galaxies presenting negative gradients, 27% with zero gradients, and 14% with positive gradients. We remark that this result does not change considerably when we consider a more restrictive definition of the zero gradient class, as $-0.05 < G < 0.05$. Moreover, essentially the same result is also obtained when we consider the whole sample, including together face and edge–on galaxies.

The total fraction of face–on barred galaxies in our sample is 79%. We can see in Table 3 that there exists an excess of barred galaxies among the ones with null or positive gradients. In (B −V), the fraction of barred galaxies with negative gradient is 75%, while it raises to 91% among the ones with zero gradient. In (U−B), 73% of the galaxies with negative gradient are barred, while 83% of the ones with null gradient are barred, and 90% of the positive gradient galaxies are barred. If we consider the more restrictive criterion for null gradient ($-0.05 < G < 0.05$), this excess is substantially emphasized. The fraction of barred galaxies with null (B −V) gradient then raises to 94% and the fraction of barred galaxies with null (U−B) gradient raises to 88%. This result indicates that barred galaxies are over–represented among the objects having null or positive gradients. Therefore, bars seem to act as a mechanism of homogenization of the color indices, and thus, of the stellar population, along galaxies. As a consequence, we are forced to conclude that a classical monolithic scenario would have difficulties to explain this result.

Another interesting feature of Table 3 is that the fraction of galaxies with AGN increase from $\sim$ 8% for systems with negative gradients to $\sim$ 36% for objects with positive gradients. Even considering the low number statistics, this might be an indication that the homogenization of the stellar population, induced by bars, is related to the AGN phenomenon.

5.3. Color Gradients and Abundances

Recent theoretical studies (e.g., Friedli & Benz 1995) related to the dynamical secular evolution show that a stellar bar is able to collect gas from the outer to the inner regions of the disk, through shocks and gravitational torques that remove angular momentum from the gas. Thus, a large–scale mixing of the gas must occur along the galaxy, which could be, in principle, observed in the radial abundance profiles of certain chemical elements. Martin & Roy (1994), hereafter MR94, and Zaritsky, Kennicutt & Huchra (1994), hereafter ZKH94, present O/H abundance gradients in spiral galaxies determined through the observation of HII regions. Both studies show that barred galaxies tend to have less pronounced gradients. Moreover, MR94 conclude that the gradients become less pronounced as the normalized length of the bar, or its apparent ellipticity, increases. On the other hand, studies from Sakamoto et al. (1999) show that barred galaxies have a higher central concentration of molecular gas (CO) than non–barred galaxies. Both results are in agreement with the prediction from the theoretical studies of dynamical secular evolution. Then, if the abundance is affected by this mechanism we also should expect it affected the color gradients.

In order to verify this possibility, we have compared 12 galaxies in common with MR94, and 18 with ZKH94. In Fig. 7, we plot our color gradients versus the abundance gradients of MR94 (top panel) and ZKH94 (bottom panel). We can see that there is no clear correlation between the photometric and the abundance gradients. Hardly this absence of correlation could be a consequence of errors in the photometric gradients, which typically range from 0.02 to 0.05. On the other hand, the errors in the abundance gradients are more difficult to determine, as we can see by looking at the quite different values of the NGC 2997 gradient as estimated by MR94 and ZKH94. However, these errors are also hardly larger than 0.02 dex $\times$ kpc^{-1} (ZKH94). One can interpret that the absence of such correlation is a real feature, and thus it is interesting to explore its consequences. Since the color indices are sensible to both age and metallicity, this result could indicate that the excess of barred galaxies with zero color gradients, as we found in Sect. 5.2, reflects a difference in the behaviour of the mean *age* of the stellar population along barred and unbarred galaxies, and not of its metallicity. However, in principle, this absence of correlation could be attributed to the effects of dust extinction. We have argued in Sect. 3.1 that these effects shall be small, but in Sect. 5.6 below we will show a quantitative analysis of these effects, and we conclude that it is possible that the lack of this correlation may be caused by dust extinction.

We would expect to find such correlation in the dynamical secular evolutionary scenario. However, if we consider that bars are a relatively fast recurrent phenomenon, this absence of

correlation would be natural. Indeed, we can imagine the following picture. If we consider a galaxy formed through the monolithic scenario, we shall expect it to show both the abundance and color gradients negative. In that case the galaxy would be placed in the lower left region of Fig. 7. This galaxy can develop a bar and then have its abundance gradient shallower, while its color gradient shall remain the same, because the time scale to mix the gas in the disk shall be smaller than the time required to form new stars in the central region. Galaxies in that stage would occupy the lower right part of Fig. 7. After the gas accumulates in the central region it will form new stars and then the color gradient will become shallower and the galaxy would be in the upper right part of Fig. 7. Instabilities generated by the mass accumulated in the central region will destroy the bar interrupting the transfer of gas along it and steepening the abundance gradient, while keeping the color gradient unchanged. In this case, we will see the galaxy in the upper left part of Fig. 7. The lack of new star formation in the central region and the aging of the stars will then turn negative the color gradient and the galaxy will again occupy the lower left part of Fig. 7. If a new bar is developed then the changes in the abundance and color gradients can occur again.

5.4. Color Gradients and the Morphology of Bars

In an attempt to perform a quantitative morphology of bars in galaxies, Martin (1995), hereafter M95, made visual estimates of the axial ratio, b/a, the major axis length (normalized by the 25 mag arcsec^{-2} isophote), L_b, and the apparent ellipticity of bars in spiral galaxies. In that work, it is found a relation between the length of the bar and the diameter of the bulge, in the sense that galaxies with large bulges also have large bars. Moreover, he found an apparent correlation between the presence of intense nuclear star formation and the axial ratio of the bar, in the sense that strong bars, those with $b/a \leq 0.6$, are present in galaxies with nuclear bursts of star formation.

A total of 45 galaxies in our sample were studied in M95, allowing us to verify correlations between our color gradients and the parameters of the bar morphology. Figure 8 shows for these objects our color gradients plotted against the bar parameters axial ratio, b/a, length, L_b, and apparent ellipticity, ε_b. We detect no correlation of these morphological bar parameters with the color gradients, meaning that the color gradient does not depend on the morphology of the bar. Thus, there are galaxies with the same gradient and bars with quite distinct morphologies. And, on the other hand, there are systems with the same bar morphology and quite different color gradients. It is worth notice that MR94 found that the O/H abundance gradients in barred galaxies turn less pronounced as the ellipticity or the length of the bar increases, i.e., galaxies with stronger bars have less pronounced O/H abundance gradients. Again, it is not unlikely that extinction by dust is masking a correlation. However, these results may be explained by different time scales in the homogenization of abundance gradients, measured in gas, and color gradients, measured in stars.

5.5. Total and Bulge Color Indices

We remark that our total color indices are obviously affected by the contributions of both the bulge and the disk. The relative importance of these two components can be measured by the factor $f_B = L_{Bb}/L_{Bd}$, representing the bulge to disk luminosity ratio in the B band. On the other hand, both components have intrinsic colors $(B-V)_d$, $(B-V)_b$ and $(U-B)_d$, $(U-B)_b$. The total color is related to these component colors through the relations

$$(B-V)_T = (B-V)_b - 2.5 \log \frac{f_B + 1}{f_B + 10^{0.4\Delta_{BV}}} \tag{8}$$

and

$$(U-B)_T = (U-B)_b + 2.5 \log \frac{f_B + 1}{f_B + 10^{-0.4\Delta_{UB}}} \tag{9}$$

where $\Delta_{BV} = (B-V)_d - (B-V)_b$ and $\Delta_{UB} = (U-B)_d - (U-B)_b$.

Table 4 shows the median values of the characteristic total and bulge color indices for the galaxies in our sample, separated by the gradient class, together with their standard errors. For those objects with null color gradient we show a single color value. In the right part of this table, we present the data relative only to the face–on objects. We can see that the same trend is present in both samples.

Considering both the face–on galaxies and the total sample, one can observe that the total colors remain almost with the same value for the three classes of gradients. The differences are small in both the (U−B) and (B −V) colors, within the errors. However, bulges of zero or positive gradient objects are systematically bluer than the ones found in negative gradient objects. The differences are much larger than the errors, indicating that it is a real effect. Indeed, there is a difference of order 0.40 magnitudes between the colors of bulges in negative and positive gradient objects, while the estimated errors are within ~ 0.03 magnitudes. Therefore, one major factor determining the value of the gradient is the bulge color. Moreover, the disk colors should also be redder, for objects with null or positive gradients, in order to keep the total colors almost unchanged, as it is observed. This is an effect which is not compatible with the monolithic scenario, since it indicates that, in the process of homogenization of the stellar population, induced by bars, bursts of star formation occur in the bulge, in complete agreement with the secular evolutionary scenario.

Another way of looking to this effect is shown in Fig. 9, where we plot the relation of the total and bulge color indices for different classes of gradients, considering only face–on galaxies. Although we have the total color instead of the disk color, these correlations have the same meaning as the ones found by other authors (Peletier & Balcells 1996), showing that the formations of bulge and disk are parts of the same process. However, this figure also shows that the zero point

scale of the correlation is quite different for objects having negative and positive color gradients. While the correlations are in the same sense, we can see again that the bulge is much bluer in objects with positive gradients, while the mean total color is the same, irrespective of the gradient category. These results do not change when we consider also the edge–on galaxies.

Once again, it is interesting to verify if there are any differences in the properties of barred and weakly–barred galaxies. Like the color gradients, the characteristic total and bulge mean color indices for SB's and SAB's are essentially the same. The bulge colors for SB's are 0.56 ± 0.02 and -0.01 ± 0.04 in (B −V) and (U−B), respectively, while for SAB's they are 0.60 ± 0.02 and 0.06 ± 0.03. On the other hand, the total colors for SB's are 0.45 ± 0.02 and -0.11 ± 0.02 in (B −V) and (U−B), and they are 0.46 ± 0.02 and -0.08 ± 0.02 for SAB's.

5.6. Dust Extinction

A fundamental point to be considered in this study are the effects of dust extinction and reddening. In principle, dust can disturb the analysis of color distribution in galaxies. To minimize its effects we have made a careful sample selection excluding galaxies presenting strong dust lanes.

Moreover, we have made our analysis considering also a sub–sample containing only the face–on galaxies of our total sample, in which it is well known that the effects of dust are minimized. We also consider the results from the models of dust distribution in disk dominated galaxies by de Jong (1996c) which show that the dust reddening plays a minor role in color gradients. This author also argues that color gradients produced by dust are small from the U to the R bands because the absorption properties do not change very much in these bands. Furthermore, we have shown that there is an excess of barred galaxies with blue bulges in comparison with non–barred galaxies, and we conclude that this is related to recent bursts of star formation. Since the effects of dust do not depend on whether or not the galaxy hosts a bar, this main conclusion remains unaltered, even if the extinction is considerable.

Nevertheless, although the extinction in face–on galaxies is smaller than in edge–on galaxies, it might be considerable in the central regions (see Peletier et al. 1995). Moreover, extinction and reddening depend on the geometry of the system and on the distribution of dust and stars (see, e.g., Jansen et al. 1994), so that it is prudent to verify empirically the role of dust in color gradients. With this aim, we have used HST archival data (NICMOS and WFPC2), and some CCD images obtained at Pico dos Dias, in order to determine the optical (B,V,I) and near–IR (H,K) color gradients for some galaxies, which are useful to evaluate the role of dust. These galaxies were chosen to have an inclination representative of our sample. As we have no photometry data in all selected passbands for all galaxies used in this analysis (see Table 5), we will assume that such gradients like $(H - K)$ indicate variations in the old stellar population, while those like $(B - V)$ or $(B - I)$ are specially sensitive to recent star formation. Color gradients like $(I - H)$ or $(V - H)$ will primarily show the extinction caused by dust, as well as old stellar

population gradients (see Peletier et al. 1999). All galaxies belong to our main sample (Sect. 2). As the HST data were measured only in the central region of the galaxies (inner $\sim$ 2 kpc), these central gradients shall not be compared with the global ones obtained in Sect. 3.

Since it is in the central region where most of the dust is accumulated, its role in color gradients evaluated here may be considered as an upper limit. Let us evaluate firstly the HST data. As the dust and gas contribution are not the same for all galaxies, we will discuss the results for each one individually, and summarize them in Table 5. NGC 3310 shows a very small old population gradient ($G(H-K) = -0.04$) and a small old population/dust gradient ($G(I-K) = -0.11$), while the color gradient produced by recent star formation is large ($G(B-I) = -0.41$). Thus one can conclude that, for this galaxy, dust may be responsible for $\sim 17\%$ of the observed central color gradient. NGC 5033 have also a very small old population gradient ($G(V-H) = +0.01$) but a *positive* and large star formation gradient ($G(B-H) = +0.39$). This means that, even with the dust present in the centre of this galaxy (as can be seen in the HST images), the blue light emitted by the young population are strong enough to produce positive color gradients. Another possibility to explain this behaviour is the presence of a strong dust lane off–centered, but this lane was not found in the images. NGC 5194 also have a very small old population gradient ($G(H-K) = -0.02$) and a considerable old population/dust gradient ($G(V-K) = -0.21$). With the star formation gradient values one can conclude that, in this galaxy, dust may cause nearly half of the observed central color gradient. Finally, NGC 5248 have a considerable old population/dust gradient ($G(V-H) = -0.24$), but a *positive* star formation gradient. Conclusions are the same as for NGC 5033.

Another way to study the role of dust in color gradients is to determine the reddening it causes. Using the HST data again we can estimate an upper limit, considering that there is no dust reddening beyond 1 R_{eff} and that there are no stellar population gradients. Thus, the difference in color from the center to 1 R_{eff} can be assumed to be all done by dust extinction. When the data does not reach 1 R_{eff} we used the farthest available radius. We thus estimated such color excesses in $(I-K)$ for NGC 3310, $(V-K)$ for NGC 5194, and $(V-H)$ and $(I-H)$ for NGC 5248. Results are in Table 5. With the Galactic extinction law Rieke & Lebofsky (1985) we have determined the extinction A_V in the centre of these galaxies. Its average value is $A_V = 1.5$. Peletier et al. 1999 applied the same analysis to a sample of early–type spirals, obtaining $A_V = 0.6 - 1.0$.

The same procedure we have used to the HST data we applied for 5 galaxies observed by us at the Pico dos Dias observatory in the B, V and I bands (see Table 5). Assuming that $(B-V)$ gradients are sensitive to recent star formation, while $(V-I)$ gradients are old population/dust gradients, we can infer the dust contribution to the observed color gradients to be of up to 45% in the central region. As one can see, there are 2 galaxies with a negative old population/dust gradients but with positive star formation gradients. This result is in agreement with the one obtained using the HST data. We have also estimated an average value for A_V using the $(V-I)$ color excesses. Its value is $A_V = 0.4$. This value is lower than the one obtained with the HST data

simply because it was not obtained with optical–near–infrared colors.

Now, assuming that the color excesses obtained truly represent an effect of dust extinction, we can "correct" the colors inside 1 R_{eff} and re–calculate the $(B-V)$ and $(U-B)$ color gradients, using the Galactic extinction law. Table 6 shows the results and compares them with the gradients determined in Sect. 3. It can be seen that, with the HST data, dust effects can, in some cases, alter significantly the color gradients determined. But in other cases, even the high values of the upper limit for A_V do not change the results. Table 6 also shows that using the color excesses obtained through our B, V and I CCD imaging make no significant changes in the color gradients.

This study has led us to conclude that indeed extinction in the center (inner $\sim$ 2 kpc) of late–type spirals is high, with a typical value for $A_V = 1-2$ magnitudes. However, the results shown here seems to indicate that dust is very much concentrated in the center, so that *global* color gradients are not much disturbed by dust, in general. The fact that, even with dust present in the center, some galaxies have positive gradients, shows that the excess of barred galaxies with blue bulges, found in this work, is a result which is not affected by our ignorance on the dust effects. It means also that, in these blue bulges, one can have an underlying old stellar population beneath a recent burst of star formation. On the other hand, it seems that the absence of correlations between color gradients and abundance gradients (Sect. 5.3), and color gradients and the bar morphology (Sect. 5.4), could possibly be explained by dust extinction.

6. General Discussion and Conclusions

In the previous section we noticed that barred galaxies have less pronounced (U−B) mean color gradients. Moreover, both at (U−B) and (B −V) the amplitude of variation of the gradient, as measured by the standard deviation of its distribution, is larger in barred, as opposed to non–barred galaxies. These results imply that there is an excess of barred galaxies among the objects with null or positive gradients, as can be seen from Table 3. As a consequence, we conclude that bars act in the sense of promoting a more homogeneous stellar population in late–type spirals. Besides an underlying old and red stellar population, disks of late–type spirals have ubiquitous young and blue stars. Bulges in general have an old stellar population, but we have shown here that bulges of late–type barred galaxies have also an important young stellar component. Therefore, the stellar population of barred galaxies tend to show a degree of mixing not compatible with the pure monolithic scenario.

We found no correlation between the color and abundance gradients. We must consider here the results of Sect. 5.6, i.e., dust extinction is considerable in the central region of late–type spirals, but does not strongly disturb global color gradients, in general. In spite of the caveat that this lack of correlation may be caused by the effects of dust, judging from the estimated photometric and abundance errors, we believe that this could be a real effect, indicating that color gradients may be not associated with metallicities (but see Peletier et al. 1999). Therefore, the

presence of color variations inside a given galaxy is quite probably related to an age effect caused by bursts of star formation. The absence of this correlation could also be explained if we consider that bars are a fast recurrent phenomenon.

Another conclusion from this study is that the mean total color indices remain remarkably constant independently of the galaxy's color gradient. From the sample of face–on objects we can verify in Table 4 that the total mean colors are $(B-V)_T \simeq 0.55 \pm 0.02$ and $(U-B)_T \simeq -0.02 \pm 0.06$. On the other hand, bulges behave quite differently. The mean colors of bulges in null gradient galaxies are ~ 0.20 bluer than the colors of bulges in negative gradient systems. Bulges of positive gradient galaxies are even bluer, ~ 0.50 bluer than bulges in negative gradient objects. We see also in Table 4 that this difference is quite too large to be explained by photometric errors. In order to keep the total color unchanged it is necessary that the disks of the null or positive gradient galaxies become redder, i.e., evolve passively.

This same effect can be clearly seen from Fig. 9, where we present the correlation between total and bulge colors. In both the negative and positive gradient regimes there is a correlation between these two colors. These correlations are in agreement with the ones found by other authors (Peletier & Balcells 1996) for the colors of bulges and disks. However, we can also see from Fig. 9 that the correlation of the positive gradient objects is shifted in the blue direction by ~ 0.50 magnitudes in their bulges. According to these authors, assuming similar metallicities for bulges and disks, their correlations imply in a difference of the order of less than 30% between the ages of the stellar populations in these two components. Again, the presence of a correlation between the total and bulge colors, as well as the bluer colors of bulges in galaxies with null or positive gradients, are not consistent with the pure monolithic scenario.

A more difficult task is to identify the correct evolutionary scenario responsible for these observable properties. The capture of nearby dwarfs in the accretion process of the hierarchical scenario seems to be incompatible with the constancy of the mean total colors of galaxies presenting different classes of color gradients, since this process do not predict a passive evolution for the disk. Moreover, the hierarchical scenario also does not predict an excess of barred galaxies showing null or positive color gradients.

On the other hand, the secular evolution induced by a bar can result in an enhancement of the star formation rate in the central regions of galaxies. This effect can be responsible for the bluer colors observed in bulges of galaxies showing null or positive color gradients. At this point we can not say, however, whether this enhancement is occurring in the bulge or in the internal region of the disk.

It is a pleasure to thank Ronaldo E. de Souza and Rob Kennicutt for fruitful discussions and suggestions, and for a careful reading of a preliminary version of the paper, and Tim Beers for presenting us the LMS method. Special thanks go to Roelof de Jong for providing us his CCD observations. We also thank G. Longo for helpful answers to our questions. We thank the

anonymous referee for helping to improve the article, specially the discussion on dust effects. We acknowledge the Conselho Nacional de Pesquisa e Desenvolvimento (CNPq), the NExGal – ProNEx and the Fundação de Amparo à Pesquisa do Estado de São Paulo (FAPESP) for the financial support. We would also like to thank the staff at the Pico dos Dias Observatory (OPD/LNA – CNPq) for helping during the observational runs.

REFERENCES

Athanassoula, E., and Bureau, M. 1999, accepted for publication in ApJ, astro-ph/9904206

Baugh, C.M., Cole, S., and Frenk, C.S. 1996, MNRAS, 283, 1361

Berentzen, I., Heller, C.H., Shlosman, I., and Fricke, K.J. 1998, MNRAS, 300, 49

Boselli, A., and Gavazzi, G. 1994, A&A, 283, 12

Bouwens, R., Cayón, L., and Silk, J. 1998, astro-ph/9812193, accepted for publication in ApJ

Bureau, M., and Athanassoula, E. 1999, accepted for publication in ApJ, astro-ph/9903061

Bureau, M., and Freeman, K.C. 1999, accepted for publication in AJ, astro-ph/9904015

Bureau, M., Freeman, K.C., and Athanassoula, E. 1999, in When and How do Bulges Form and Evolve?, ed. by C.M. Carollo, H.C. Ferguson & R.F.G. Wyse, Cambridge: CUP, astro-ph/9901246

Combes, F., and Sanders, R.H. 1981, A&A, 96, 164

Courteau, S., de Jong, R., and Broeils, A. 1996, ApJ, 457, L73

de Jong, R.S. 1996a, A&A, 118, 557

de Jong, R.S. 1996b, A&A, 313, 45

de Jong, R.S. 1996c, A&A, 313, 377

de Jong, R.S., and van der Kruit, P.C. 1994, A&A, 106, 451

de Souza, R.E., and dos Anjos, S. 1987, A&A, 70, 465

de Vaucouleurs, G. 1959, AJ, 64, 397

de Vaucouleurs, G., de Vaucouleurs, A., Corwin, H.G., Buta, R.J., Paturel, G., and Fouque P. 1991, in: Third Reference Catalog of Bright Galaxies, Springer–Verlag, New York **(RC3)**

Eggen, O.J., Lynden–Bell, D., and Sandage, A.R. 1962, ApJ, 136, 748

Elmegreen, D.M. 1998, in Galaxies and Galactic Structure, Prentice Hall

Evans, R. 1994, MNRAS, 266, 511

Friedli, D. 1999, in The Evolution of Galaxies on Cosmological Timescales, ed. by J.E. Beckman & T.J. Mahoney, ASP Conf. Ser., astro-ph/9903143

Friedli, D., and Benz, W. 1995, A&A, 301, 649

Friedli, D., and Martinet, L. 1993, A&A, 277, 27

Frogel, J.A. 1985, ApJ, 298, 528

Giovanelli, R., Haynes, M.P., Salzer, J.J., Wegner, G., da Costa, L.N., and Freudling, W., 1994, AJ, 107(6), 2036

Giovanelli, R., Haynes, M.P., Salzer, J.J., Wegner, G., da Costa, L.N., and Freudling, W., 1995, AJ, 110(3), 1059

Graham, J.A. 1982, PASP, 94, 244

Jansen, R.A. et al. 1994, MNRAS, 270, 343

Kauffmann, G., and White, S.D.M. 1993, MNRAS, 261, 921

Kauffmann, G., Guiderdoni, B., and White, S.D.M. 1994, MNRAS, 267, 981

Kitchin, C.R. 1998, in Astrophysical Techniques, Institute of Physics Publishing, Bristol and Philadelphia

Kormendy, J. 1982, ApJ, 257, 75

Kormendy, J., and Illingworth, G. 1983, ApJ, 265, 632

Kuijken, K., and Merrifield, M.R. 1995, ApJ, 443, L13

Lahav, O., Naim, A, Buta, R.J., Corwin, H.G., and de Vaucouleurs, G. et al. 1995, Science, 267, 859

Larson, R.B., and Tinsley, B.M. 1978, ApJ, 219, 46

Longo, G., and de Vaucouleurs, A. 1983, Univ. Texas Monographs in Astronomy, No. 3 **(LdV83)**

Longo, G., and de Vaucouleurs, A. 1985, Univ. Texas Monographs in Astronomy, No. 3A **(LdV85)**

Martin, P. 1995, AJ, 109(6), 2428 **(M95)**

Martin, P., and Roy, J.R. 1994, ApJ, 424, 599 **(MR94)**

Merrifield, M.R., and Kuijken, K. 1999, A&A, 345, L47

Norman, C.A., Sellwood, J.A., and Hasan, H. 1996, ApJ, 462, 114

Peletier, R.F. 1989, PhD Thesis, University of Groningen, The Netherlands

Peletier, R.F., and Balcells, M. 1996, AJ, 111, 2238

Peletier, R.F., Valentjin, E.A., Moorwood, A.F.M., and Freudling, W. 1994, A&A, 108, 621

Peletier, R.F. et al. 1995, A&A, 300, L1

Peletier, R.F. et al. 1999, MNRAS, 310, 703

Prugniel, Ph., and Héraudeau, Ph. 1998, A&A, 128, 299 **(PH98)**

Rieke, G., Lebofsky, M.J. 1985, ApJ, 288, 618

Roberts, M.S., and Haynes, M.P. 1994, ARA&A, 32, 115

Rousseeuw, P.J. 1984, Journal of the American Statistical Association, 79(388), 871

Rousseeuw, P.J., and Leroy, A.M. 1987, in: Robust Regression and Outlier Detection, Wiley–Interscience, New York

Sakamoto, K., Okumura, S.K., Ishizuki, S., and Scoville, N.Z. 1999, in When and How do Bulges Form and Evolve?, ed. by C.M. Carollo, H.C. Ferguson & R.F.G. Wyse, Cambridge University Press, astro-ph/9902005

Schlegel, D.J., Finkbeiner, D.P., and Davis, M. 1998, ApJ, 500, 525

Shlosman, I., Begelman, M.C., and Frank, J. 1990, Nature, 345, 679

Shlosman, I., Frank, J., and Begelman, M.C. 1989, Nature, 338, 45

Searle, L., Sargent, W.L.W., and Bagnuolo, W.G. 1973, ApJ, 179, 427

Shaw, M.A. 1987, MNRAS, 229, 691

Silva, D.R., and Elston, R. 1994, ApJ, 428, 511

Tinsley, B.M. 1980, Fund. of Cos. Phys., 5, 287

Toomre, A. 1966, in Geophysical Fluid Dynamics, 1966 Summer Study Program at Woods Hole Oceanographic Institution, ref. no. 66-46, 111

van den Bergh, S. 1997, AJ, 113, 2054

Véron–Cetty, M.P., and Véron, P. 1998, in: Quasars and Active Galactic Nuclei (8th Ed.), ESO Sci. Rep., 18, 1

Wyse, R.F.G., Gilmore, G., and Franx, M. 1997, ARA&A, 35, 637

Zaritsky, D., Kennicutt, R.C., and Huchra, J.P. 1994, ApJ, 420, 87 **(ZKH94)**

Fig. 1.— Examples of color gradients. Filled boxes indicate the (B −V), while circles indicate the (U−B). The color indices in magnitudes are plotted against the decimal logarithm of the aperture in units of 0.1 arcminute. Dashed lines refer to the LS method, while dotted lines refer to the LMS method and the solid lines refer to the PROGRESS algorithm.

Fig. 2.— Color gradients for the galaxies in our sample plotted against the color excess ($E(B-V)$) caused by Galactic reddening (top panels), and against the inclination of the galaxy ($\log R_{25}$ parameter of RC3 – bottom panels – the most edge–on galaxies are at the right side). The absence of correlations show that we can neglect the effects of Galactic and internal reddening when calculating color gradients in galaxies. Typical error bars are drawn at the bottom–right of each panel.

Fig. 3.— Comparison between color gradients determined through photoelectric aperture photometry data (LdV) and through surface photometry (CCD). The good correlation shown atest the validity of the results obtained here.

Fig. 4.— Comparison between color gradients from PH98 and from this work. The dashed line indicates a one–by–one correlation. The solid line indicates a linear fit.

Fig. 5.— Distribution of the (B −V) and (U−B) color gradients determined for the galaxies in our sample. (a): non–barred face–on galaxies; (b): barred face–on galaxies; (c): non–barred edge–on galaxies and (d): barred edge–on galaxies.

Fig. 6.— The (U−B) gradients plotted against the (B −V) gradients for: (a) non–barred galaxies, (b): barred galaxies and (c): all sample. The straight line corresponds to a linear fit.

Fig. 7.— Correlation between our photometric gradients and the O/H abundance gradients of MR94 (top panel) and ZKH94 (bottom panel). Boxes indicate the (B −V) gradient, while circles indicate the (U−B). Filled symbols refer to barred galaxies. In the bottom right part of each panel typical error bars are shown.

Fig. 8.— Color gradients plotted against the morphological parameters of the bars of M95. In the top panels the gradients are plotted against the axial ratio. In the middle panels they are plotted against the normalized length of the bars, while in the bottom panels a correlation with the apparent ellipticity was sought.

Fig. 9.— The correlation for the total and bulge characteristic color indices, calculated through our first method, for galaxies with negative color gradients (upper panels) and positive color gradients (lower panels). The solid lines are fits to the data points. The fits of the upper panels are also shown in the lower panels (dotted lines) for comparison. Only face–on galaxies are considered.

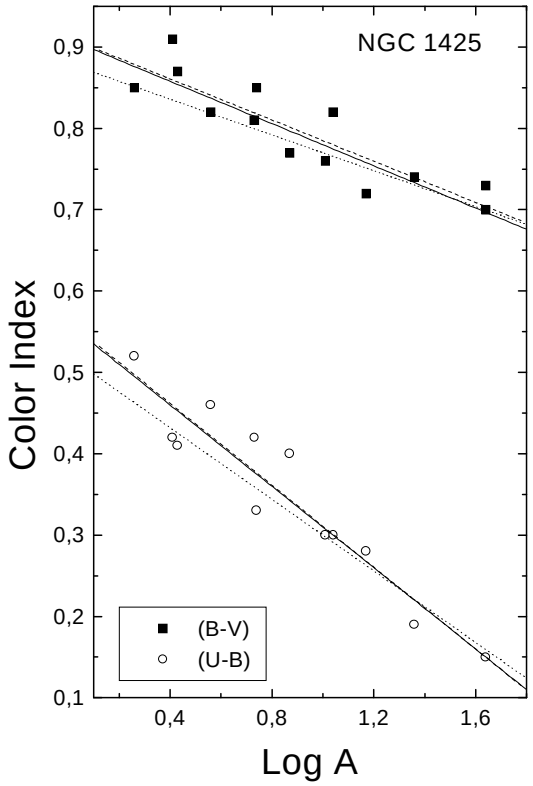
NGC 1425
Color Index
Log A
(B-V)
(U-B)

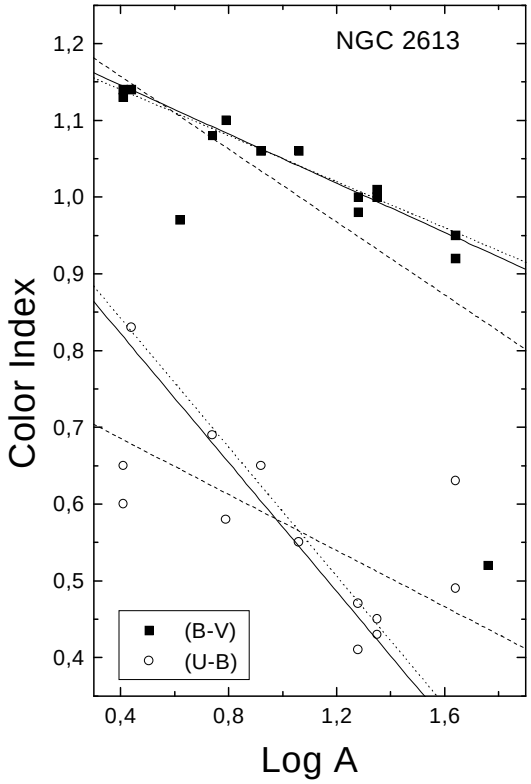
NGC 2613
Color Index
Log A
(B-V)
(U-B)

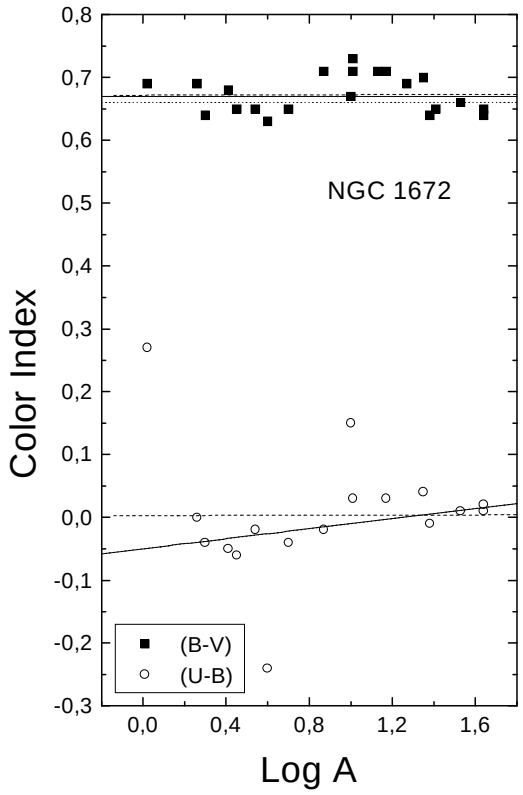
NGC 1672
Color Index
Log A
(B-V)
(U-B)

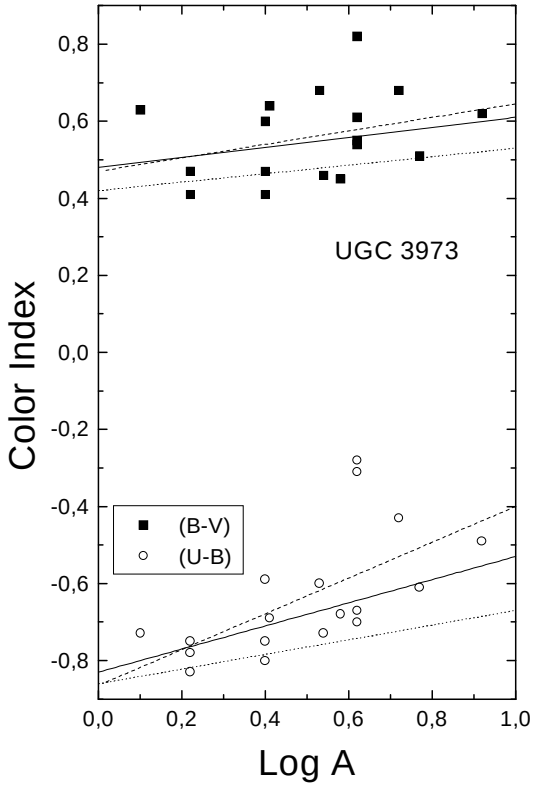
UGC 3973
Color Index
Log A
(B-V)
(U-B)

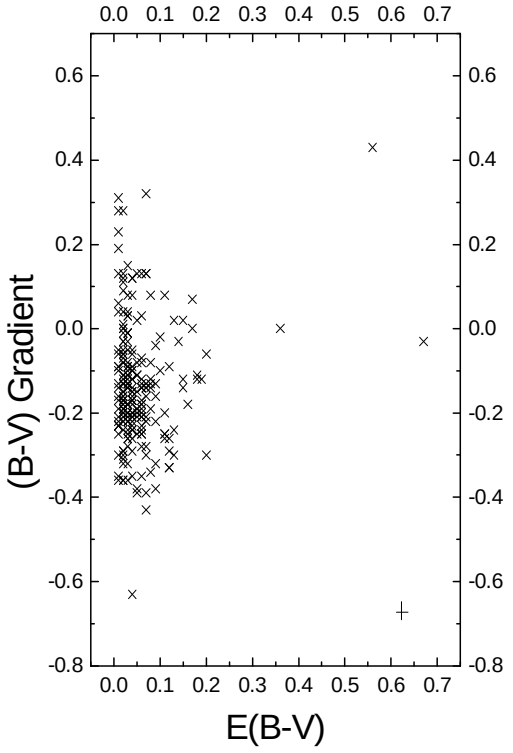
(B-V) Gradient
E(B-V)

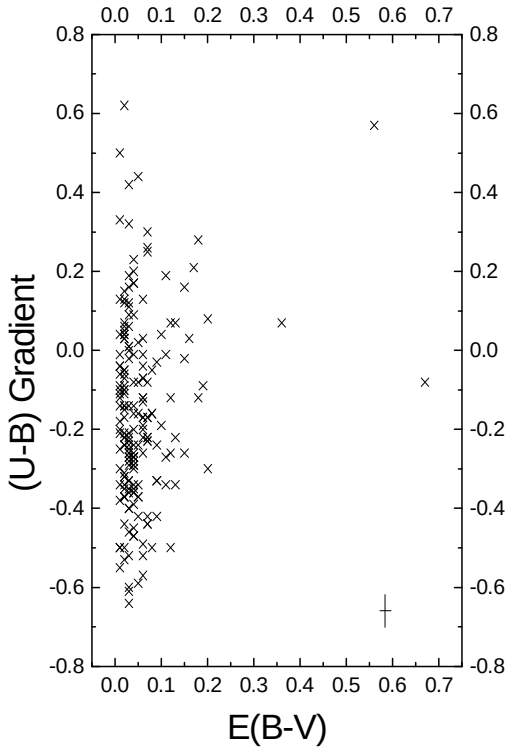
(U-B) Gradient
E(B-V)

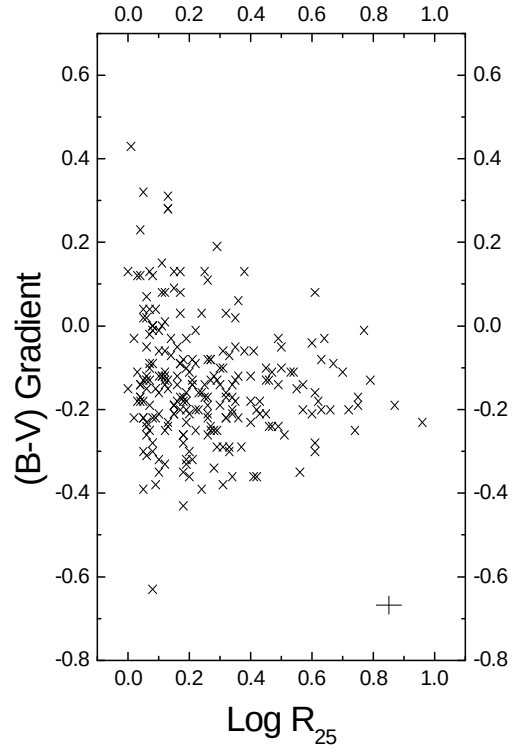
(B-V) Gradient
Log R25

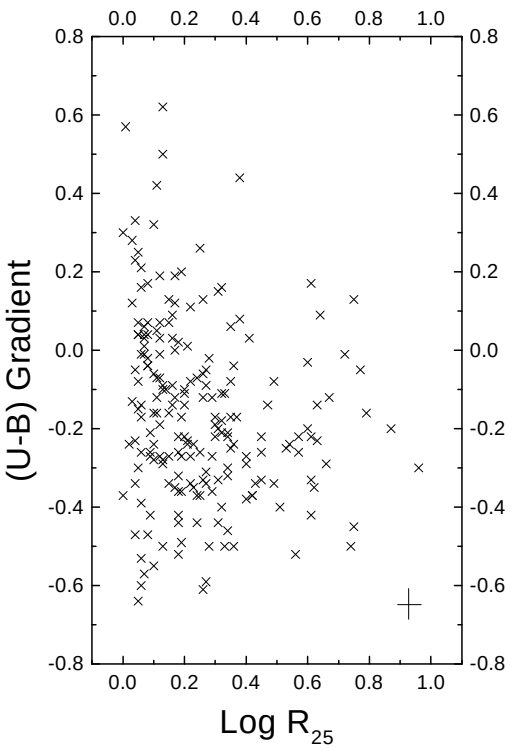
(U-B) Gradient
Log R25

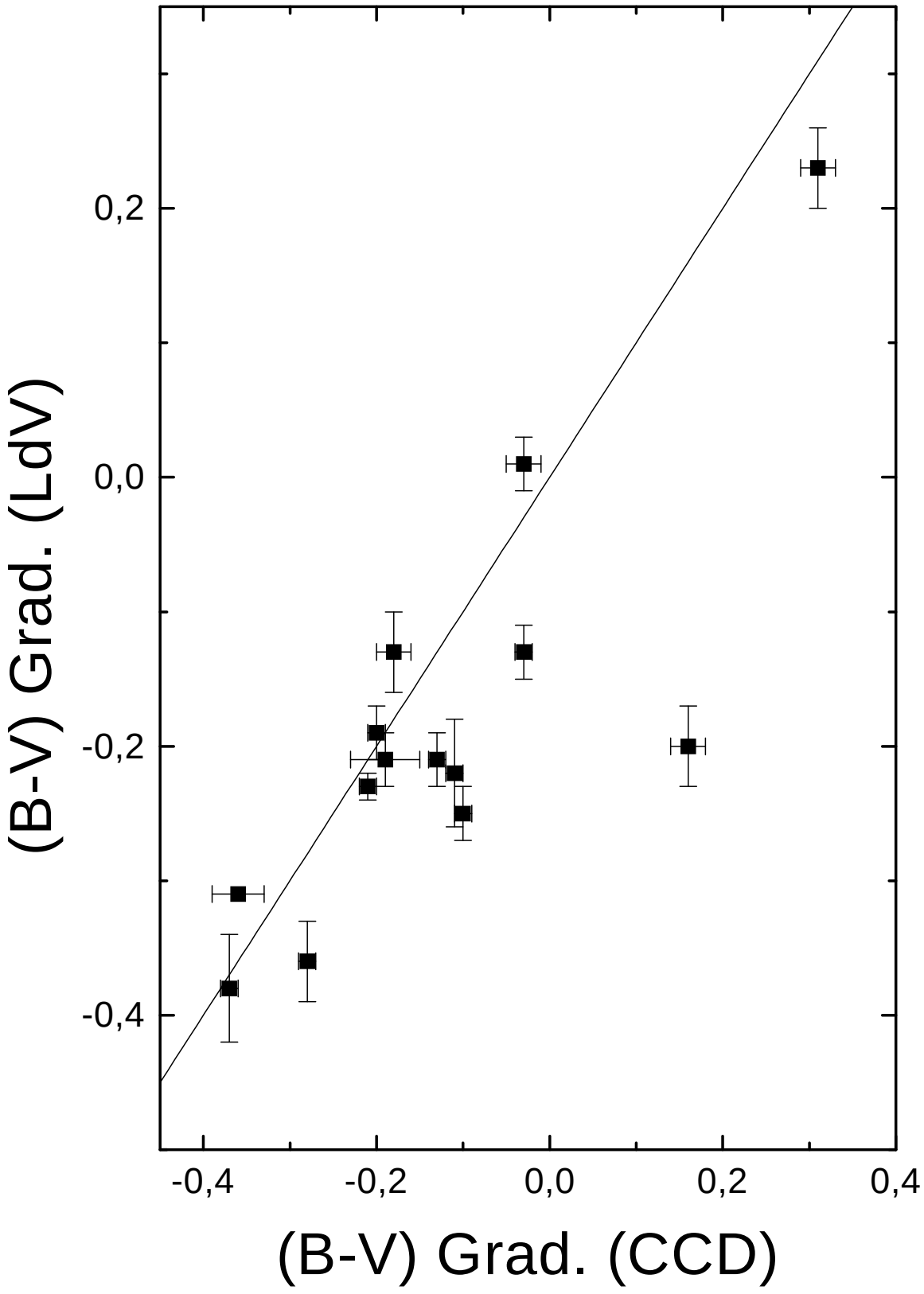
0,2
0,0
-0,2
-0,4
(B-V) Grad. (LdV)
-0,4
-0,2
0,0
0,2
0,4
(B-V) Grad. (CCD)

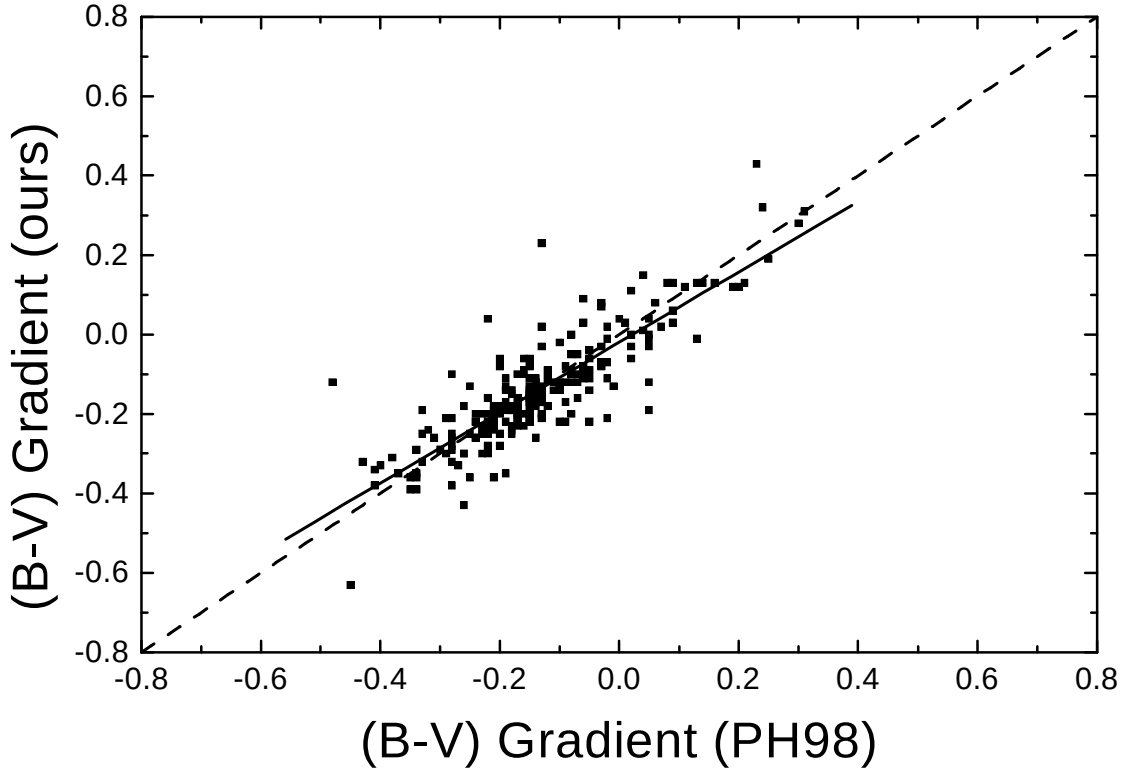
(B-V) Gradient (ours)
(B-V) Gradient (PH98)
0.8
0.6
0.4
0.2
0.0
-0.2
-0.4
-0.6
-0.8
-0.8
-0.6
-0.4
-0.2
0.0
0.2
0.4
0.6
0.8

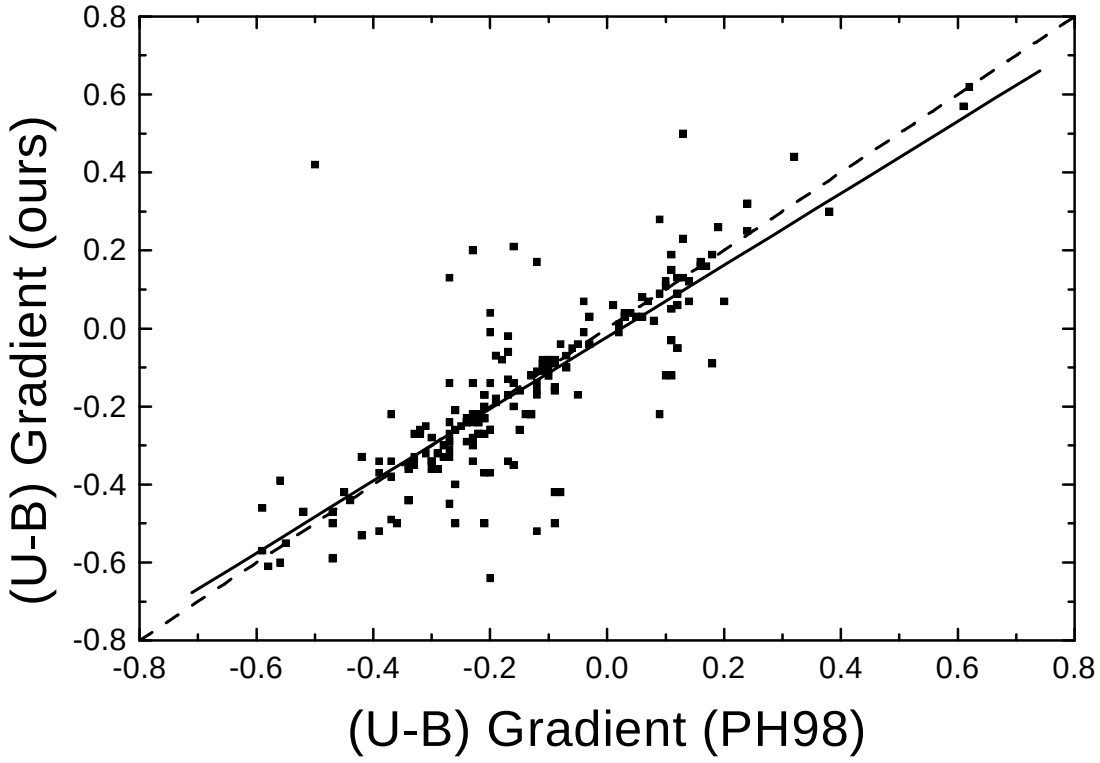
(U-B) Gradient (ours)
(U-B) Gradient (PH98)
0.8
0.6
0.4
0.2
0.0
-0.2
-0.4
-0.6
-0.8
-0.8
-0.6
-0.4
-0.2
0.0
0.2
0.4
0.6
0.8

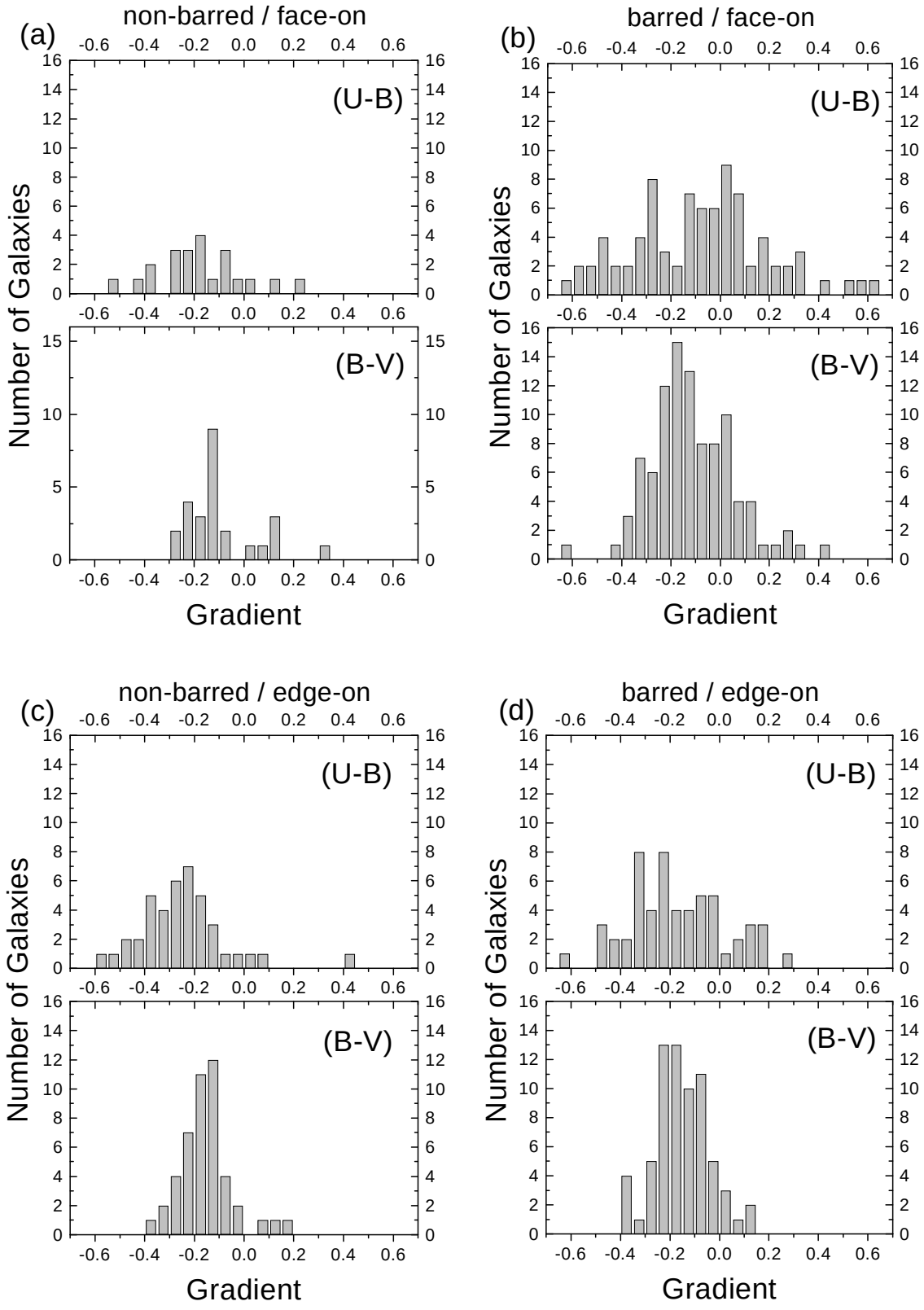
(a)
non-barred / face-on
(b)
barred / face-on
(c)
non-barred / edge-on
(d)
barred / edge-on
(U-B)
(B-V)
Number of Galaxies
Gradient

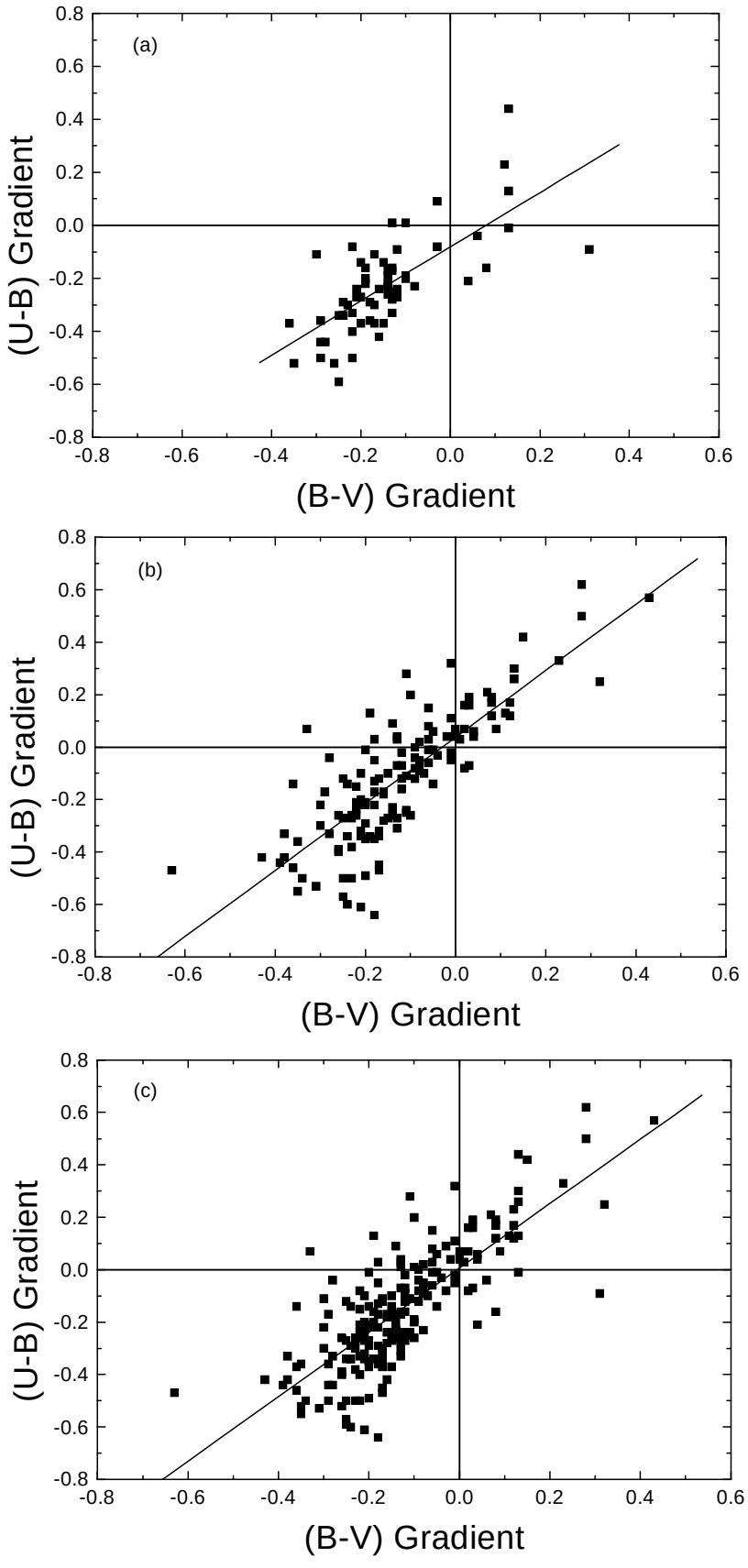
(a)
(U-B) Gradient
(B-V) Gradient
(b)
(U-B) Gradient
(B-V) Gradient
(c)
(U-B) Gradient
(B-V) Gradient

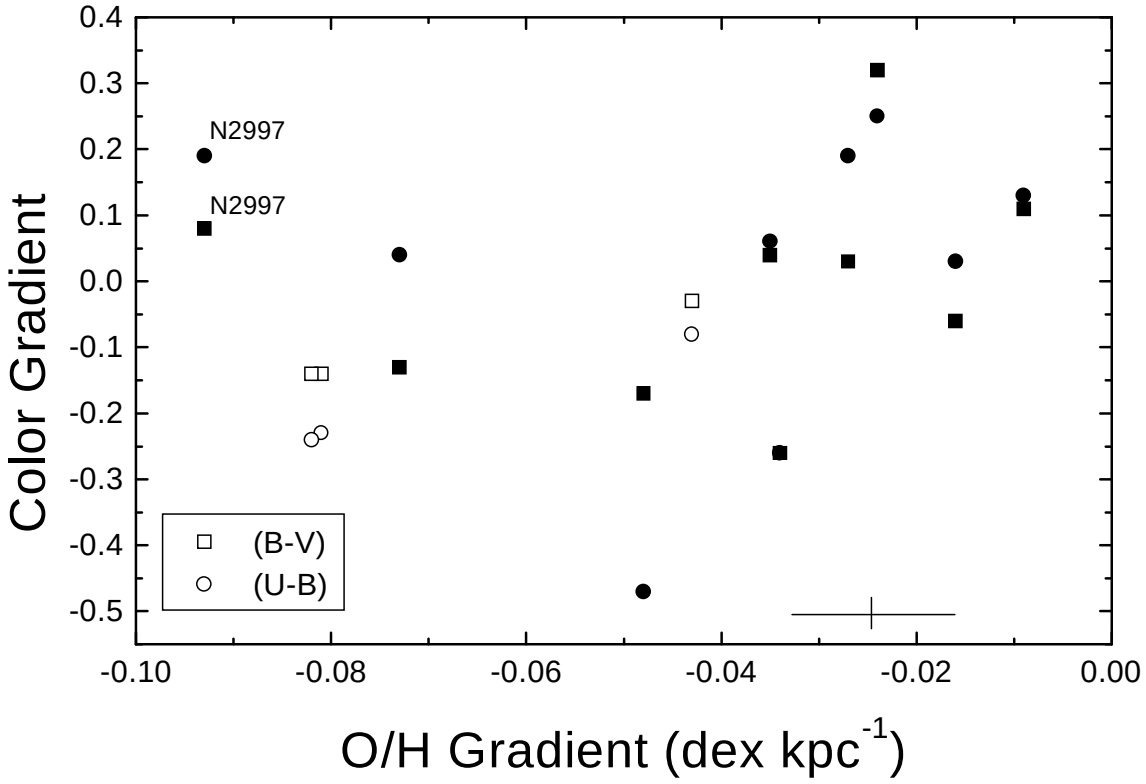
N2997
N2997
(B-V)
(U-B)
Color Gradient
O/H Gradient (dex kpc-1)
0.4
0.3
0.2
0.1
0.0
-0.1
-0.2
-0.3
-0.4
-0.5
-0.10
-0.08
-0.06
-0.04
-0.02
0.00

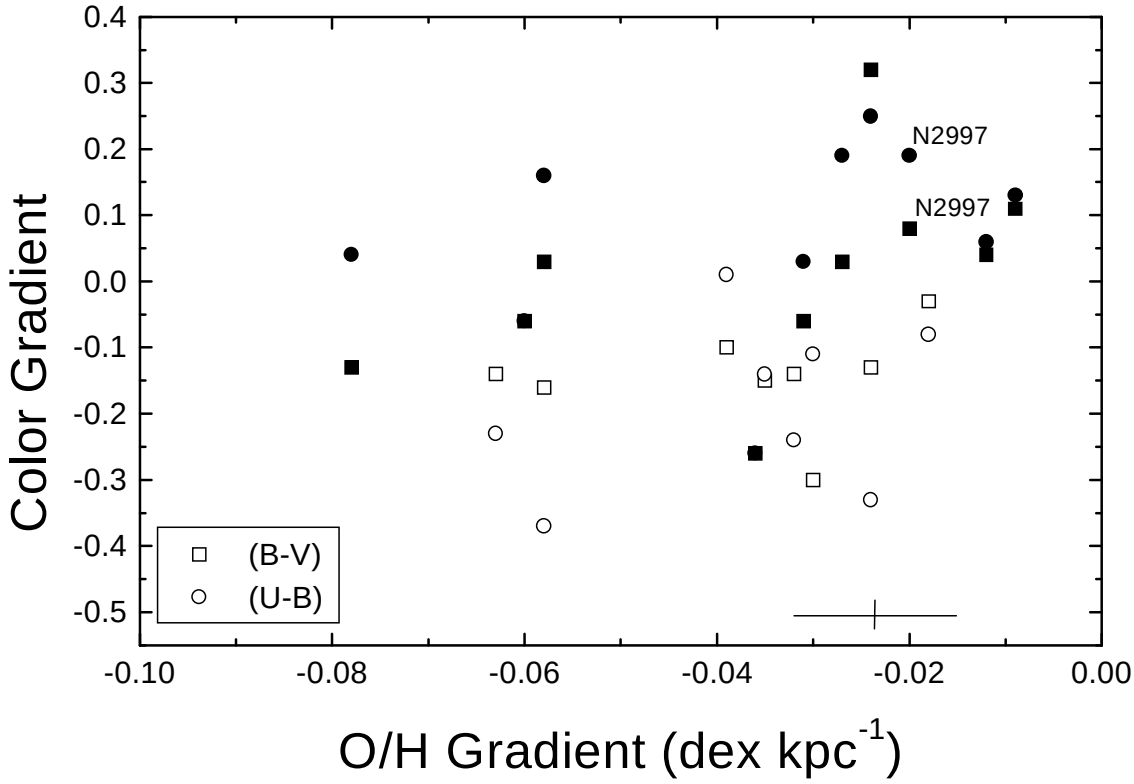
N2997
N2997
(B-V)
(U-B)
Color Gradient
O/H Gradient (dex kpc-1)
0.4
0.3
0.2
0.1
0.0
-0.1
-0.2
-0.3
-0.4
-0.5
-0.10
-0.08
-0.06
-0.04
-0.02
0.00

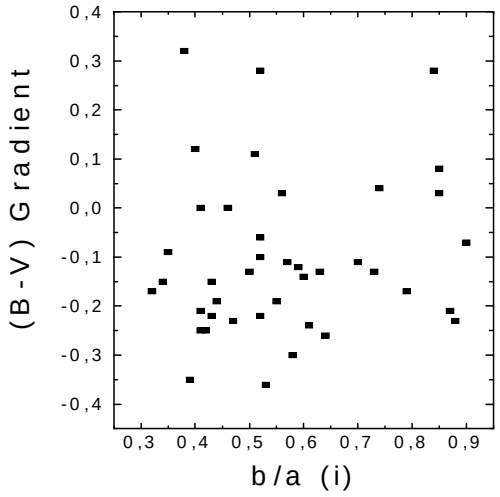
(B-V) Gradient
b/a (i)

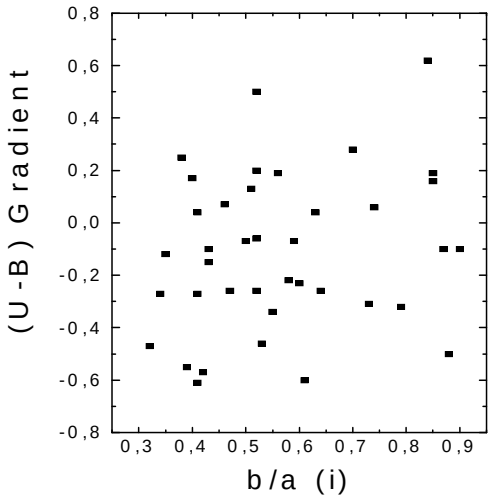
(U-B) Gradient
b/a (i)

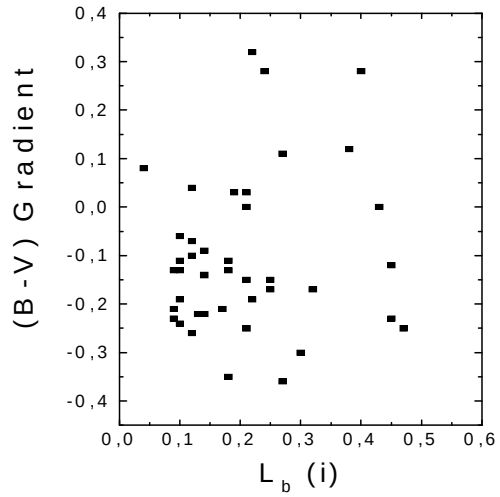
(B-V) Gradient
L b (i)

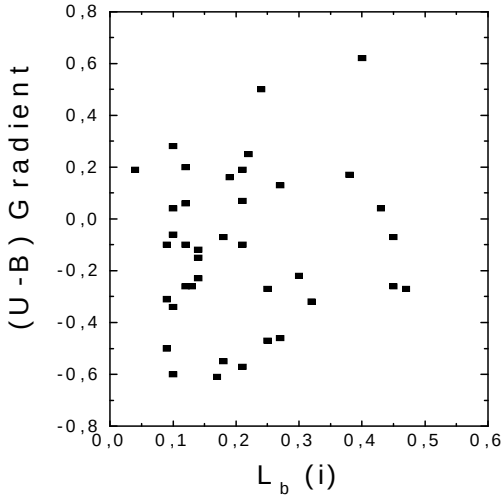
(U-B) Gradient
L b (i)

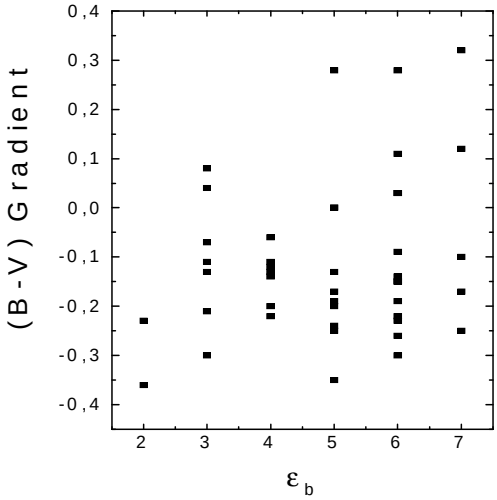
(B-V) Gradient
ε b

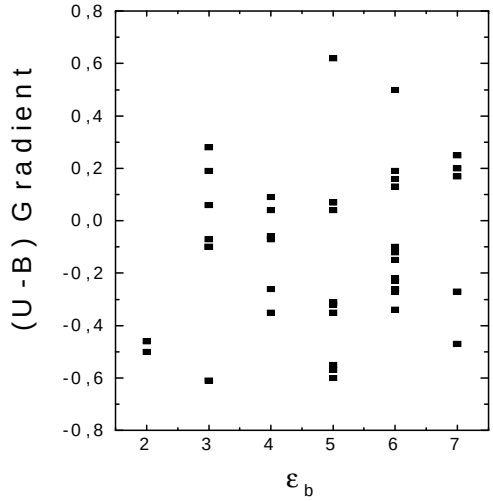
(U-B) Gradient
ε b

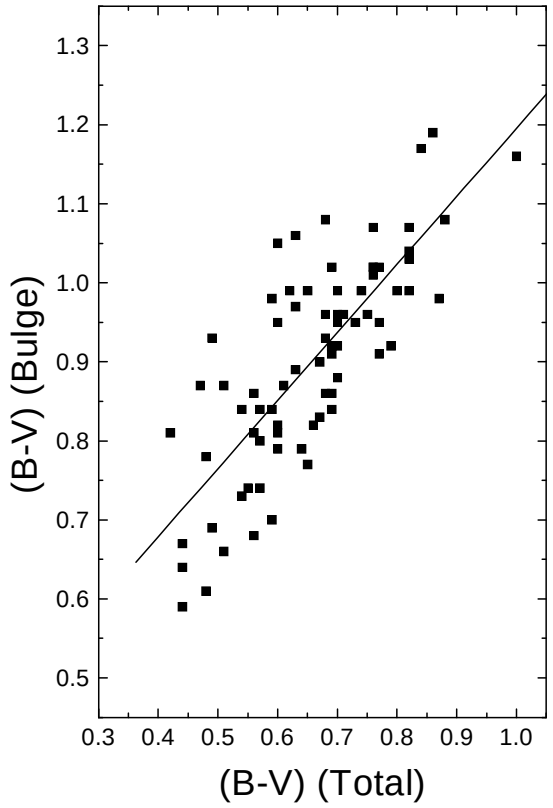
(B-V) (Bulge)
(B-V) (Total)
1.3
1.2
1.1
1.0
0.9
0.8
0.7
0.6
0.5
0.3 0.4 0.5 0.6 0.7 0.8 0.9 1.0

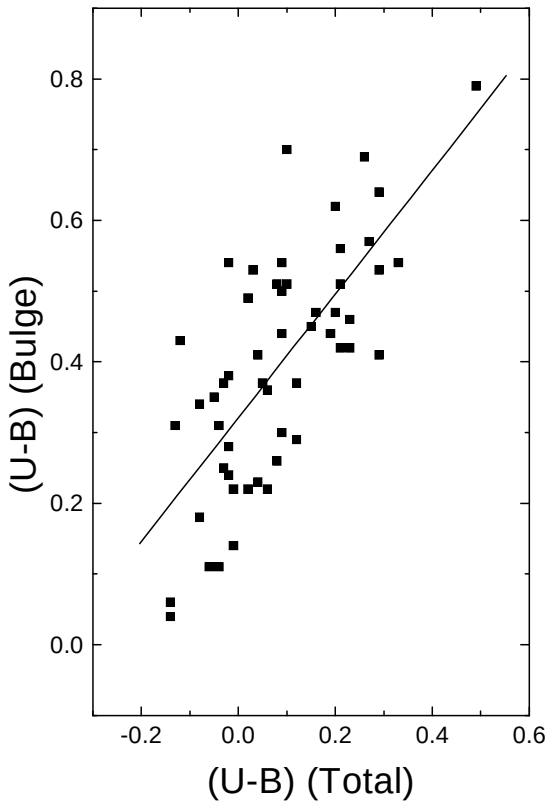
(U-B) (Bulge)
(U-B) (Total)
0.8
0.6
0.4
0.2
0.0
-0.2 0.0 0.2 0.4 0.6

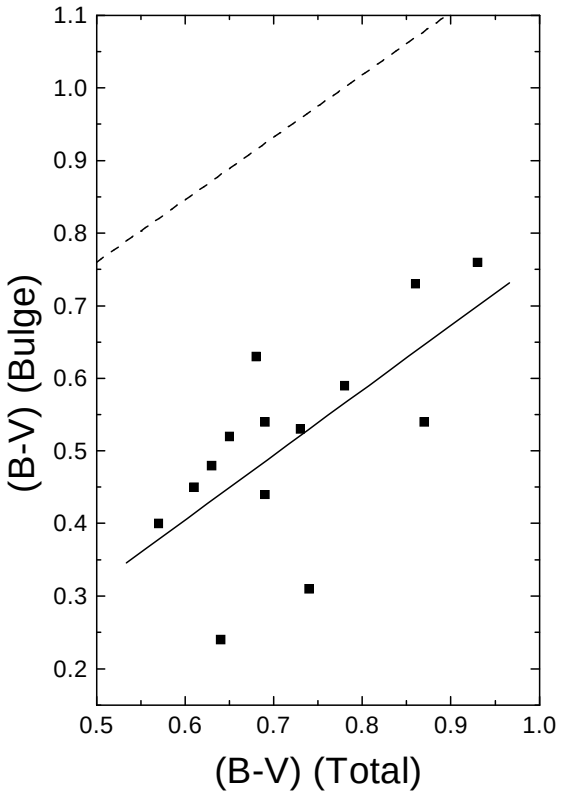
(B-V) (Bulge)
(B-V) (Total)
1.1
1.0
0.9
0.8
0.7
0.6
0.5
0.4
0.3
0.2
0.5 0.6 0.7 0.8 0.9 1.0

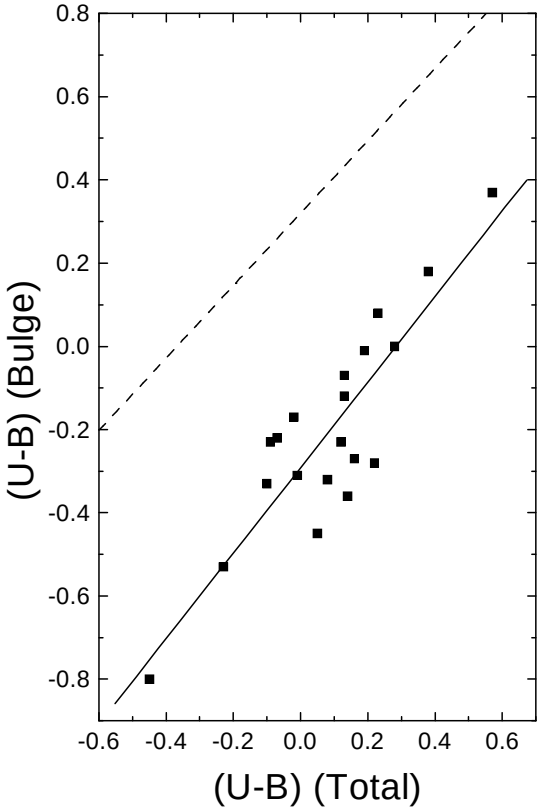
(U-B) (Bulge)
(U-B) (Total)
0.8
0.6
0.4
0.2
0.0
-0.2
-0.4
-0.6
-0.8
-0.6 -0.4 -0.2 0.0 0.2 0.4 0.6

Table 1. The sample.

Name (1)	Type (2)	$G(B-V)$ (3)	error (4)	$G(U-B)$ (5)	error (6)	$(B-V)_b$ (7)	$(B-V)_T$ (8)	$(U-B)_b$ (9)	$(U-B)_T$ (10)
ESO271-010	SABcd(s)	-0,02	0,03	0,04	0,06	0,39	0,39	-0,22	-0,22
IC0342	SABcd(rs)	0,43	0,08	0,57	0,09	0,23	0,66	-0,51	0,06
IC1954	SBb(s)	-0,06	0,03	0,15	0,10	0,24	0,24	-0,40	-0,25
IC1993	SABb(rs)	-0,05	0,03	-0,01	0,10	0,73	0,73	0,24	0,24
IC2554	SBbc(s)	-0,06	0,03	0,08	0,04	0,19	0,19	-0,45	-0,45
IC4444	SABbc(rs)	0,00	0,03	–	–	0,40	0,40	–	–
IC4839	SAbc(s)	-0,28	0,03	-0,44	0,06	0,88	0,60	0,41	-0,03
IC4845	Sb(rs)	0,13	0,00	-0,01	0,07	0,45	0,58	0,05	0,05
IC4852	SBbc(s)	-0,13	0,05	0,03	0,07	0,67	0,54	-0,07	-0,07
IC5092	SBc(rs)	-0,01	0,03	-0,02	0,09	0,69	0,69	0,09	0,09
IC5179	Sbc(rs)	-0,17	0,04	-0,11	0,03	0,46	0,29	-0,12	-0,23
IC5186	SABb(rs)	-0,11	0,01	-0,11	0,04	0,53	0,42	-0,06	-0,17
IC5325	SABbc(rs)	-0,18	0,03	-0,05	0,05	0,69	0,51	-0,07	-0,07
MCG-2-14-4	SABcd(rs)	-0,33	0,11	0,07	0,01	0,64	0,31	-0,11	-0,11
NGC0001	Sb	-0,14	0,01	-0,19	0,05	0,76	0,62	0,19	0,00
NGC0024	Sc(s)	-0,20	0,06	-0,14	0,06	0,29	0,09	-0,33	-0,47
NGC0134	SABbc(s)	-0,18	0,01	-0,35	0,03	0,49	0,31	0,12	-0,23
NGC0150	SBb(rs)	-0,22	0,00	-0,21	0,04	0,54	0,32	-0,05	-0,26
NGC0151	SBbc(r)	-0,36	0,03	-0,46	0,06	0,73	0,37	0,33	-0,13
NGC0157	SABbc(rs)	-0,23	0,03	-0,27	0,04	0,60	0,37	0,07	-0,20
NGC0210	SABb(s)	-0,17	0,02	-0,32	0,00	0,78	0,61	0,30	-0,02
NGC0224	Sb(s)	-0,03	0,00	-0,08	0,01	-0,10	-0,10	-0,26	-0,26
NGC0278	SABb(rs)	-0,03	0,04	–	–	0,51	0,51	–	–
NGC0289	SBbc(rs)	-0,19	0,02	-0,34	0,02	0,78	0,59	0,32	-0,02
NGC0309	SABc(r)	-0,63	0,04	-0,47	0,10	0,91	0,28	0,26	-0,21
NGC0440	Sbc(s)	-0,16	0,02	-0,24	0,06	0,51	0,35	-0,03	-0,27
NGC0470	Sb(rs)	-0,13	0,03	0,01	0,06	0,63	0,50	-0,06	-0,06
NGC0488	Sb(r)	-0,13	0,02	-0,28	0,04	0,90	0,77	0,58	0,30
NGC0578	SABc(rs)	-0,21	0,03	-0,10	0,01	0,50	0,29	-0,15	-0,25
NGC0613	SBbc(rs)	0,01	0,02	0,03	0,04	0,63	0,63	0,06	0,06
NGC0615	Sb(rs)	-0,12	0,01	-0,27	0,02	0,55	0,43	0,29	0,02
NGC0628	Sc(s)	-0,14	0,01	-0,23	0,02	0,64	0,50	0,09	-0,14
NGC0685	SABc(r)	-0,22	0,03	-0,15	0,04	0,62	0,40	-0,04	-0,19
NGC0779	SABb(r)	-0,11	0,02	-0,25	0,03	0,45	0,34	0,10	-0,16
NGC0782	SBb(r)	-0,31	0,00	-0,53	0,06	0,82	0,51	0,44	-0,09
NGC0864	SABc(rs)	-0,11	0,03	–	–	0,55	0,44	–	–
NGC0908	Sc(s)	-0,22	0,02	-0,50	0,04	0,54	0,32	0,17	-0,33
NGC0958	SBc(rs)	-0,13	0,04	–	–	0,48	0,35	–	–
NGC1055	SBb	-0,10	0,02	-0,26	0,04	0,53	0,43	0,13	-0,13
NGC1068	Sb(rs)	-0,10	0,01	0,01	0,01	0,74	0,64	0,00	0,00
NGC1073	SBc(rs)	-0,17	0,03	-0,47	0,04	0,62	0,45	0,22	-0,25
NGC1084	Sc(s)	-0,14	0,04	-0,26	0,01	0,50	0,36	0,03	-0,23
NGC1087	SABc(rs)	-0,01	0,04	0,11	0,04	0,31	0,31	-0,36	-0,25
NGC1097	SBb(s)	0,08	0,03	0,12	0,02	0,64	0,64	0,03	0,15
NGC1187	SBc(r)	-0,15	0,02	-0,10	0,04	0,60	0,45	-0,01	-0,11
NGC1232	SABc(rs)	-0,24	0,01	-0,60	0,04	0,79	0,55	0,45	-0,15
NGC1255	SABbc(rs)	-0,36	0,02	-0,14	0,04	0,62	0,26	-0,10	-0,24
NGC1288	SABc(rs)	-0,30	0,02	–	–	0,88	0,58	–	–
NGC1300	SBbc(rs)	-0,18	0,03	-0,22	0,03	0,71	0,53	0,21	-0,01
NGC1365	SBb(s)	0,11	0,02	0,13	0,04	0,43	0,54	-0,16	-0,03
NGC1421	SABbc(rs)	-0,30	0,02	-0,22	0,03	0,24	-0,06	-0,28	-0,50
NGC1425	Sb(s)	-0,13	0,02	-0,25	0,02	0,51	0,38	0,13	-0,12
NGC1483	SBbc(s)	-0,09	0,04	-0,04	0,04	0,39	0,39	-0,26	-0,26
NGC1515	SABbc(s)	-0,09	0,02	-0,12	0,01	0,33	0,33	-0,05	-0,17
NGC1530	SBb(rs)	-0,12	0,04	-0,02	0,01	0,55	0,43	-0,11	-0,11
NGC1536	SBc(s)	-0,03	0,10	–	–	0,51	0,51	–	–
NGC1566	SABbc(s)	-0,06	0,03	-0,06	0,05	0,57	0,57	-0,04	-0,04
NGC1614	SBc(s)	0,02	0,03	0,16	0,04	0,44	0,44	-0,34	-0,18
NGC1620	SABbc(rs)	-0,24	0,01	–	–	0,56	0,32	–	–
NGC1637	SABc(rs)	-0,22	0,04	-0,26	0,06	0,76	0,54	0,18	-0,08
NGC1672	SBb(s)	0,00	0,01	0,04	0,01	0,57	0,57	-0,05	-0,05

Table 1—Continued

Name (1)	Type (2)	$G(B-V)$ (3)	error (4)	$G(U-B)$ (5)	error (6)	$(B-V)_b$ (7)	$(B-V)_T$ (8)	$(U-B)_b$ (9)	$(U-B)_T$ (10)
NGC1688	SBd(rs)	0,15	0,04	0,42	0,12	0,30	0,45	-0,44	-0,02
NGC1703	SBb(r)	-0,18	0,00	-0,64	0,00	0,69	0,51	0,36	-0,28
NGC1784	SBc(r)	-0,30	0,00	-0,22	0,05	0,81	0,51	0,24	0,02
NGC1792	Sbc(rs)	-0,19	0,03	-0,22	0,04	0,51	0,32	-0,06	-0,28
NGC1796	SBc(rs)	-0,08	0,01	-0,09	0,04	0,31	0,31	-0,26	-0,26
NGC1832	SBbc(r)	-0,43	0,02	-0,42	0,06	0,77	0,34	0,19	-0,23
NGC1888	SBc(s)	-0,14	0,05	-0,26	0,05	0,43	0,29	0,11	-0,15
NGC1961	SABc(rs)	-0,33	0,09	–	–	0,73	0,40	–	–
NGC2082	SBb(r)	-0,18	0,03	-0,13	0,06	0,67	0,49	-0,08	-0,21
NGC2090	Sc(rs)	-0,10	0,02	-0,20	0,03	0,61	0,51	0,17	-0,03
NGC2206	SABbc(rs)	-0,25	0,05	–	–	0,66	0,41	–	–
NGC2207	SABbc(rs)	-0,32	0,03	–	–	0,64	0,32	–	–
NGC2223	SABb(r)	-0,25	0,02	-0,57	0,08	0,88	0,63	0,54	-0,03
NGC2268	SABbc(r)	-0,08	0,02	–	–	0,53	0,53	–	–
NGC2336	SABbc(r)	-0,21	0,03	-0,61	0,05	0,60	0,39	0,37	-0,24
NGC2339	SABbc(rs)	-0,12	0,02	–	–	0,75	0,63	–	–
NGC2347	Sb(r)	-0,19	0,03	–	–	0,76	0,57	–	–
NGC2389	SABc(rs)	-0,21	0,08	–	–	0,55	0,34	–	–
NGC2417	Sbc(rs)	-0,12	0,03	-0,09	0,08	0,62	0,50	0,00	0,00
NGC2442	SABbc(s)	-0,30	0,02	-0,30	0,01	0,86	0,56	0,34	0,04
NGC2487	SBb	-0,38	0,03	-0,42	0,08	0,93	0,55	0,41	-0,01
NGC2512	SBb	-0,08	0,01	0,02	0,05	0,54	0,54	-0,05	-0,05
NGC2565	SBbc	0,02	0,01	-0,08	0,12	0,52	0,52	0,07	0,07
NGC2595	SABc(rs)	-0,06	0,02	-0,01	0,02	0,60	0,60	0,07	0,07
NGC2608	SBb(s)	-0,09	0,06	-0,08	0,07	0,53	0,53	-0,06	-0,06
NGC2613	Sb(s)	-0,16	0,01	-0,42	0,04	0,47	0,31	0,28	-0,14
NGC2683	Sb(rs)	-0,08	0,01	-0,23	0,02	0,34	0,34	0,07	-0,16
NGC2712	SBb(r)	-0,19	0,03	–	–	0,63	0,44	–	–
NGC2715	SABc(rs)	-0,11	0,06	–	–	0,27	0,16	–	–
NGC2776	SABc(rs)	0,04	0,05	0,04	0,05	0,52	0,52	-0,11	-0,11
NGC2815	SBb(r)	-0,24	0,02	-0,34	0,07	0,60	0,36	0,37	0,03
NGC2841	Sb(r)	-0,12	0,01	-0,24	0,03	0,68	0,56	0,36	0,12
NGC2874	SBbc(r)	-0,26	0,04	-0,40	0,04	0,62	0,36	0,23	-0,17
NGC2889	SABc(rs)	-0,26	0,02	-0,39	0,10	0,87	0,61	0,37	-0,02
NGC2903	SABbc(rs)	0,03	0,02	0,16	0,03	0,40	0,40	-0,24	-0,08
NGC2935	SABb(s)	-0,12	0,05	-0,07	0,10	0,76	0,64	0,13	0,13
NGC2955	Sb(r)	0,19	0,07	–	–	0,21	0,40	–	–
NGC2964	SABbc(r)	-0,08	0,04	-0,06	0,01	0,49	0,49	-0,18	-0,18
NGC2989	SABbc(s)	-0,17	0,03	-0,12	0,00	0,42	0,25	-0,16	-0,28
NGC2997	SABc(rs)	0,08	0,02	0,19	0,03	0,68	0,68	0,01	0,20
NGC3001	SABbc(rs)	-0,09	0,06	-0,12	0,06	0,58	0,58	0,02	-0,10
NGC3054	SABb(r)	-0,14	0,02	-0,23	0,03	0,74	0,60	0,26	0,03
NGC3079	SBc(s)	-0,25	0,01	-0,50	0,07	0,31	0,06	0,02	-0,48
NGC3095	SABc(rs)	-0,39	0,03	-0,44	0,05	0,67	0,38	0,19	-0,25
NGC3124	SABbc(rs)	-0,19	0,03	–	–	0,80	0,61	–	–
NGC3145	SBbc(rs)	-0,25	0,01	-0,12	0,12	0,72	0,47	0,18	0,06
NGC3177	Sb(rs)	0,04	0,02	-0,21	0,05	0,54	0,54	0,51	0,30
NGC3223	Sb(s)	-0,25	0,00	-0,34	0,04	0,76	0,50	0,36	0,02
NGC3281	Sab(s)	-0,10	0,01	-0,19	0,06	0,74	0,64	0,31	0,12
NGC3289	SB0+(rs)	-0,04	0,03	-0,03	0,02	0,31	0,31	-0,01	-0,01
NGC3310	SABbc(r)	0,00	0,01	0,05	0,04	0,19	0,19	-0,54	-0,54
NGC3318	SABb(rs)	-0,34	0,02	-0,50	0,04	0,58	0,24	0,13	-0,37
NGC3333	SABbc	-0,19	0,04	0,13	0,15	0,20	0,01	-0,55	-0,42
NGC3347	SBb(rs)	0,03	0,01	-0,07	0,02	0,61	0,61	0,16	0,16
NGC3351	SBb(r)	0,03	0,02	0,19	0,05	0,66	0,66	-0,03	0,16
NGC3353	Sb	0,13	0,06	0,13	0,05	0,17	0,30	-0,57	-0,44
NGC3390	Sb	-0,13	0,02	-0,16	0,08	0,32	0,19	-0,06	-0,22
NGC3521	SABbc(rs)	-0,07	0,03	–	–	0,52	0,52	–	–
NGC3627	SABb(s)	-0,20	0,02	-0,21	0,02	0,62	0,42	0,18	-0,03
NGC3628	Sb	-0,11	0,04	–	–	0,28	0,17	–	–
NGC3689	SABc(rs)	0,13	0,10	–	–	0,37	0,50	–	–
NGC3810	Sc(rs)	-0,21	0,06	-0,27	0,07	0,64	0,43	0,08	-0,19

Table 1—Continued

Name (1)	Type (2)	$G(B-V)$ (3)	error (4)	$G(U-B)$ (5)	error (6)	$(B-V)_b$ (7)	$(B-V)_T$ (8)	$(U-B)_b$ (9)	$(U-B)_T$ (10)
NGC4051	SABbc(rs)	0,28	0,04	0,50	0,05	0,37	0,65	-0,44	0,06
NGC4088	SABbc(rs)	-0,36	0,01	–	–	0,55	0,19	–	–
NGC4096	SABc(rs)	-0,20	0,05	-0,22	0,03	0,32	0,12	-0,15	-0,37
NGC4156	SBb(rs)	-0,01	0,08	0,32	0,17	0,72	0,72	-0,31	0,01
NGC4216	SABb(s)	-0,20	0,02	-0,29	0,03	0,59	0,39	0,35	0,06
NGC4254	Sc(s)	-0,15	0,01	-0,14	0,00	0,64	0,49	0,06	-0,08
NGC4258	SABbc(s)	-0,06	0,03	0,03	0,06	0,39	0,39	-0,04	-0,04
NGC4273	SBc(s)	-0,03	0,09	–	–	0,33	0,33	–	–
NGC4303	SABbc(rs)	-0,13	0,03	0,04	0,07	0,65	0,52	-0,01	-0,01
NGC4321	SABbc(s)	0,04	0,01	0,06	0,06	0,61	0,61	-0,04	-0,04
NGC4388	Sb(s)	-0,03	0,01	0,09	0,01	0,17	0,17	-0,34	-0,34
NGC4414	Sc(rs)	-0,17	0,01	-0,37	0,15	0,75	0,58	0,38	0,01
NGC4501	Sb(rs)	-0,24	0,01	-0,34	0,03	0,76	0,52	0,36	0,02
NGC4527	SABbc(s)	-0,24	0,03	-0,14	0,05	0,68	0,44	0,08	-0,06
NGC4535	SABc(s)	0,09	0,02	0,07	0,09	0,53	0,53	-0,06	-0,06
NGC4536	SABbc(rs)	-0,29	0,02	-0,17	0,06	0,54	0,25	-0,08	-0,25
NGC4548	SBb(rs)	-0,16	0,03	-0,28	0,01	0,87	0,71	0,49	0,21
NGC4565	Sb	-0,19	0,02	-0,20	0,07	0,32	0,13	0,06	-0,14
NGC4579	SABb(rs)	-0,12	0,01	-0,16	0,02	0,84	0,72	0,41	0,25
NGC4593	SBb(rs)	0,28	0,11	0,62	0,03	0,65	0,93	-0,40	0,22
NGC4647	SABc(rs)	-0,32	0,12	–	–	0,83	0,51	–	–
NGC4651	Sc(rs)	-0,26	0,00	-0,52	0,00	0,73	0,47	0,34	-0,18
NGC4666	SABc	-0,15	0,00	–	–	0,42	0,27	–	–
NGC4699	SABb(rs)	-0,05	0,01	-0,14	0,02	0,75	0,75	0,41	0,27
NGC4900	SBc(rs)	0,12	0,01	0,12	0,09	0,42	0,54	-0,27	-0,15
NGC4902	SBb(r)	-0,39	0,09	–	–	0,94	0,56	–	–
NGC4911	SABbc(r)	-0,17	0,06	-0,34	0,01	0,86	0,69	0,41	0,07
NGC4939	Sbc(s)	-0,29	0,02	-0,36	0,06	0,70	0,41	0,24	-0,12
NGC5005	SABbc(rs)	-0,16	0,03	-0,18	0,02	0,69	0,53	0,29	0,11
NGC5033	Sc(s)	-0,30	0,03	-0,11	0,06	0,65	0,35	0,15	0,04
NGC5055	Sbc(rs)	-0,16	0,01	-0,37	0,06	0,68	0,52	0,19	-0,18
NGC5188	SABb(s)	-0,21	0,10	-0,34	0,06	0,62	0,41	0,19	-0,15
NGC5194	Sbc(s)	-0,14	0,01	-0,24	0,02	0,58	0,44	0,04	-0,20
NGC5236	SABc(s)	0,32	0,01	0,25	0,04	0,47	0,79	-0,20	0,05
NGC5248	SABbc(rs)	-0,07	0,02	-0,10	0,03	0,58	0,58	0,06	-0,04
NGC5364	Sbc(rs)	-0,18	0,02	-0,36	0,03	0,67	0,49	0,24	-0,12
NGC5371	SABbc(rs)	-0,35	0,03	-0,55	0,04	0,91	0,56	0,51	-0,04
NGC5426	Sc(s)	-0,22	0,04	-0,33	0,10	0,53	0,31	0,00	-0,33
NGC5427	Sc(s)	-0,09	0,00	–	–	0,52	0,52	–	–
NGC5483	Sc(s)	-0,14	0,03	–	–	0,63	0,49	–	–
NGC5530	Sbc(rs)	-0,29	0,04	-0,50	0,02	0,74	0,45	0,50	0,00
NGC5592	SBbc(s)	-0,08	0,01	-0,05	0,05	0,52	0,52	-0,04	-0,04
NGC5633	Sb(rs)	-0,32	0,15	–	–	0,70	0,38	–	–
NGC5643	SABc(rs)	0,07	0,14	0,21	0,08	0,58	0,58	-0,10	0,11
NGC5653	Sb(rs)	0,31	0,10	-0,09	0,07	0,24	0,55	-0,12	-0,12
NGC5676	Sbc(rs)	-0,22	0,02	-0,40	0,02	0,59	0,37	0,20	-0,20
NGC5746	SABb(rs)	-0,17	0,04	-0,45	0,10	0,46	0,29	0,29	-0,16
NGC5792	SBb(rs)	-0,21	0,02	-0,20	0,00	0,47	0,26	0,01	-0,19
NGC5850	SBb(r)	-0,23	0,04	-0,26	0,05	0,90	0,67	0,45	0,19
NGC5859	SBbc(s)	-0,05	0,06	–	–	0,40	0,40	–	–
NGC5861	SABc(rs)	-0,26	0,06	–	–	0,68	0,42	–	–
NGC5879	Sbc(rs)	-0,14	0,02	–	–	0,36	0,22	–	–
NGC5899	SABc(rs)	-0,18	0,06	–	–	0,59	0,41	–	–
NGC5907	Sc(s)	-0,23	0,01	-0,30	0,04	0,17	-0,06	-0,21	-0,51
NGC5921	SBbc(r)	-0,15	0,02	-0,27	0,02	0,73	0,58	0,23	-0,04
NGC5962	Sc(r)	-0,19	0,04	-0,16	0,06	0,66	0,47	0,11	-0,05
NGC5970	SBc(r)	-0,17	0,00	–	–	0,71	0,54	–	–
NGC5985	SABb(r)	-0,13	0,02	-0,31	0,03	0,67	0,54	0,27	-0,04
NGC5987	Sb	-0,10	0,04	–	–	0,63	0,53	–	–
NGC6052	Sc	0,08	0,03	-0,16	0,03	0,18	0,18	0,20	-0,54
NGC6181	SABc(rs)	-0,18	0,02	-0,17	0,03	0,49	0,31	-0,12	-0,29
NGC6207	Sc(s)	0,06	0,02	-0,04	0,02	0,20	0,20	-0,39	-0,39

Table 1—Continued

Name (1)	Type (2)	$G(B-V)$ (3)	error (4)	$G(U-B)$ (5)	error (6)	$(B-V)_b$ (7)	$(B-V)_T$ (8)	$(U-B)_b$ (9)	$(U-B)_T$ (10)
NGC6217	SBbc(rs)	0,12	0,04	0,17	0,03	0,40	0,52	-0,31	-0,14
NGC6221	SBc(s)	-0,18	0,02	0,03	0,03	0,62	0,44	-0,06	-0,06
NGC6239	SBb(s)	-0,05	0,02	0,06	0,03	0,18	0,18	-0,39	-0,39
NGC6384	SABbc(r)	-0,26	0,03	-0,26	0,04	0,70	0,44	0,28	0,02
NGC6412	Sc(s)	-0,12	0,03	–	–	0,57	0,45	–	–
NGC6574	SABbc(rs)	-0,12	0,03	-0,12	0,06	0,67	0,55	0,10	-0,02
NGC6643	Sc(rs)	-0,14	0,01	-0,17	0,05	0,49	0,35	-0,10	-0,27
NGC6699	SABbc(rs)	-0,22	0,02	-0,24	0,04	0,76	0,54	0,14	-0,10
NGC6744	SABbc(r)	-0,10	0,03	0,20	0,09	0,71	0,61	0,40	0,60
NGC6753	Sb(r)	-0,13	0,02	-0,17	0,03	0,86	0,73	0,24	0,07
NGC6764	SBbc(s)	0,13	0,06	0,26	0,06	0,32	0,45	-0,35	-0,09
NGC6769	SABb(r)	-0,20	0,03	-0,49	0,13	0,76	0,56	0,42	-0,07
NGC6780	SABc(rs)	-0,28	0,10	-0,04	0,07	0,76	0,48	0,01	0,01
NGC6814	SABbc(rs)	-0,11	0,05	0,28	0,13	0,82	0,71	-0,06	0,22
NGC6872	SBb(s)	-0,11	0,02	-0,24	0,03	0,52	0,39	0,31	0,07
NGC6887	Sbc	-0,20	0,07	-0,37	0,09	0,52	0,32	0,16	-0,21
NGC6890	Sb(rs)	-0,21	0,02	-0,24	0,04	0,82	0,61	0,24	0,00
NGC6923	SBb(rs)	-0,38	0,04	-0,33	0,04	0,76	0,38	0,23	-0,10
NGC6925	Sbc(s)	-0,35	0,02	-0,52	0,12	0,55	0,20	0,23	-0,29
NGC6951	SABbc(rs)	0,00	0,05	0,07	0,07	0,62	0,62	0,10	0,10
NGC6984	SBc(r)	-0,35	0,03	-0,36	0,01	0,62	0,27	0,06	-0,30
NGC7038	SABc(s)	-0,13	0,03	-0,27	0,03	0,63	0,50	0,25	-0,02
NGC7083	Sbc(s)	-0,20	0,02	-0,27	0,02	0,63	0,43	0,13	-0,14
NGC7090	SBc	-0,01	0,06	-0,05	0,01	-0,11	-0,11	-0,59	-0,59
NGC7125	SABc(rs)	-0,14	0,01	0,09	0,09	0,36	0,22	-0,20	-0,20
NGC7126	Sc(rs)	-0,17	0,02	-0,30	0,05	0,49	0,32	0,01	-0,29
NGC7137	SABc(rs)	0,02	0,01	0,07	0,02	0,51	0,51	-0,12	-0,12
NGC7171	SBb(rs)	-0,20	0,01	-0,35	0,05	0,67	0,47	0,15	-0,20
NGC7177	SABb(r)	-0,16	0,02	-0,17	0,02	0,76	0,60	0,33	0,16
NGC7184	SBc(r)	-0,28	0,01	-0,33	0,09	0,50	0,22	0,11	-0,22
NGC7205	Sbc(s)	-0,29	0,01	-0,44	0,02	0,60	0,31	0,11	-0,33
NGC7314	SABbc(rs)	-0,21	0,02	-0,32	0,05	0,54	0,33	0,01	-0,31
NGC7329	SBb(r)	-0,20	0,04	-0,35	0,01	0,78	0,58	0,38	0,03
NGC7331	Sb(s)	-0,13	0,01	-0,33	0,04	0,57	0,44	0,25	-0,08
NGC7339	SABbc(s)	0,08	0,11	0,17	0,03	0,32	0,32	-0,37	-0,20
NGC7412	SBb(s)	-0,23	0,01	-0,50	0,03	0,64	0,41	0,29	-0,21
NGC7448	Sbc(rs)	-0,14	0,02	-0,22	0,00	0,30	0,16	-0,17	-0,39
NGC7479	SBc(s)	-0,25	0,02	-0,27	0,02	0,78	0,53	0,30	0,03
NGC7496	SBb(s)	0,23	0,03	0,33	0,06	0,35	0,58	-0,42	-0,09
NGC7531	SABbc(r)	-0,23	0,01	-0,38	0,02	0,60	0,37	0,19	-0,19
NGC7537	Sbc	-0,22	0,03	-0,08	0,04	0,30	0,08	-0,42	-0,42
NGC7541	SBbc(rs)	-0,21	0,04	-0,22	0,05	0,45	0,24	-0,10	-0,32
NGC7590	Sbc(rs)	-0,36	0,03	-0,37	0,10	0,55	0,19	0,05	-0,32
NGC7606	Sb(s)	-0,18	0,04	-0,29	0,08	0,57	0,39	0,11	-0,18
NGC7640	SBc(s)	-0,20	0,02	-0,01	0,02	0,02	-0,18	-0,59	-0,59
NGC7673	Sc	0,12	0,04	0,23	0,14	0,19	0,31	-0,58	-0,35
NGC7716	SABb(r)	-0,22	0,03	–	–	0,81	0,59	–	–
NGC7723	SBb(r)	-0,09	0,04	0,00	0,05	0,58	0,58	0,00	0,00
NGC7742	Sb(r)	-0,15	0,05	-0,37	0,20	0,79	0,63	0,32	-0,05
NGC7755	SBc(rs)	-0,13	0,03	-0,07	0,04	0,74	0,61	0,05	0,05
NGC7757	Sc(rs)	-0,24	0,07	-0,29	0,12	0,51	0,27	-0,07	-0,36
NGC7782	Sb(s)	-0,25	0,06	-0,59	0,19	0,82	0,56	0,51	-0,08
UGC03973	SBb	0,13	0,10	0,30	0,07	0,30	0,43	-1,02	-0,72
UGC04013	Sb	0,13	0,05	0,44	0,12	0,13	0,26	-1,08	-0,64

Note. — Columns (1) and (2) show, respectively, the name and the morphological type of the galaxy, according to the RC3. Columns (3) and (4) show the (B −V) gradient and its error, while columns (5) and (6) do that for the (U−B) gradient. Columns (7) and (8) show the (B −V) bulge and total color indices, respectively, whereas columns (9) and (10) do that for the (U−B) gradient.

Table 2. Total number of galaxies, mean values and standard deviations for the distributions presented in Fig. 5.

Description (1)	N (2)	mean value (3) G(B −V)	SD (4)	N (5)	mean value (6) G(U−B)	SD (7)
(a) non–barred face–on galaxies	26	-0.14 ± 0.01	0.06	22	-0.19 ± 0.03	0.14
(b) barred face–on galaxies	98	-0.14 ± 0.02	0.15	82	-0.08 ± 0.03	0.27
(c) non–barred edge–on galaxies	46	-0.16 ± 0.01	0.07	41	-0.26 ± 0.02	0.12
(d) barred edge–on galaxies	68	-0.16 ± 0.01	0.10	56	-0.19 ± 0.03	0.20

Table 3. Distribution of the face–on galaxies in our sample in relation to the gradient categories to be analysed.

	Color	Total (1)	Sample (2)	SA (3)	SAB (4)	SB (5)	SAB+SB (6)	AGN (7)
G $\geq$ 0.1	(B-V)	14	11%	28%	29%	43%	72%	5(36%)
-0.1 < G < 0.1		32	26%	9%	53%	38%	91%	4(12%)
G $\leq$ -0.1		78	63%	25%	47%	28%	75%	8(10%)
G $\geq$ 0.1	(U-B)	19	18%	10%	37%	53%	90%	7(37%)
-0.1 < G < 0.1		30	29%	17%	53%	30%	83%	2(7%)
G $\leq$ -0.1		55	53%	27%	42%	31%	73%	4(7%)

Note. — (1): total number of galaxies in the category; (2): fraction of the total sample in the category; (3): fraction of non–barred galaxies; (4): fraction of weakly–barred galaxies; (5): fraction of barred galaxies; (6): total fraction of barred galaxies; (7): galaxies with AGN.

Table 4. Median values for the total and bulge characteristic color indices for the galaxies in our sample, separated in relation to the gradient categories. The values for the whole sample are shown in the left part of the table, while those for the face–on objects are in the right.

	Color	Bulge	Total	Color	Bulge	Total
		Total Sample			Face–on	
G $\geq$ 0.1	(B −V)	0.34±0.03	0.53±0.04	(B −V)	0.36±0.03	0.55±0.05
-0.1 $<$ G $<$ 0.1		0.52±0.03	0.52±0.03		0.57±0.02	0.57±0.02
G $\leq$ -0.1		0.64±0.01	0.43±0.01		0.74±0.01	0.53±0.01
G $\geq$ 0.1	(U−B)	-0.35±0.06	-0.08±0.05	(U−B)	-0.31±0.07	0.05±0.07
-0.1 $<$ G $<$ 0.1		-0.06±0.03	-0.06±0.03		-0.05±0.03	-0.05±0.03
G $\leq$ -0.1		0.19±0.02	-0.14±0.01		0.24±0.03	-0.05±0.02

Table 5. Color gradients and excesses for the galaxies in the dust extinction studies.

Galaxy G(I-H)	G(B-V) G(I-K)	G(B-I) G(H-K)	G(B-H) E(V-I)	G(B-K) E(V-H)	G(V-I) E(V-K)	G(V-H) E(I-H)	G(V-K) E(I-K)
NGC 3310		-0.41					
-0.11	-0.11	-0.04					0.42
NGC 5033	+0.01		+0.39			+0.01	
NGC 5194	-0.40		-0.50	-0.47			-0.21
		-0.02			1.41		
NGC 5248					+0.20	-0.24	
-0.38				0.68		0.75	
NGC 782	-0.36				-0.10		
			0.11				
NGC 6769	+0.16				-0.18		
			0.25				
NGC 6890	-0.19				-0.06		
			0.04				
NGC 6923	-0.37				-0.28		
			0.31				
NGC 7496	+0.31				-0.30		
			0.22				

Table 6. Comparison between the color gradients with (right) and without (left) internal extinction correction.

Galaxy	$G(B-V)_0$	$G(B-V)_c$	$G(U-B)_0$	$G(U-B)_c$
NGC 3310	0.00	+0.26	+0.05	0.35
NGC 5194	-0.14	-0.12	-0.24	+0.09
NGC 5248	-0.07	+0.11	-0.10	-0.05
NGC 782	-0.31	-0.28	-0.53	-0.47
NGC 6769	-0.20	-0.19	-0.49	-0.42
NGC 6890	-0.21	-0.18	-0.24	-0.09
NGC 6923	-0.38	-0.38	-0.33	-0.22
NGC 7496	+0.23	+0.23	+0.33	+0.40